(19) Europäisch[illegible]atentamt
European P[illegible]nt Offic
Offic uropé n des brev ts

(11) EP 0 757 392 A1

(12) EUROPEAN PATENT APPLICATION

(43) Date of publication:
05.02.1997 Bulletin 1997/06

(21) Application number: **96305577.7**

(22) Date of filing: **30.07.1996**

(51) Int Cl.[6]: **H01L 29/868**, H01L 31/075, H01L 29/12, H01L 29/864, H01L 29/737, H01L 29/778

(84) Designated Contracting States:
DE FR GB NL

(30) Priority: **03.08.1995 EP 95305436**

(71) Applicant: **HITACHI EUROPE LIMITED**
Maidenhead, Berkshire, SL6 8YA (GB)

(72) Inventor: **Allam, Jeremy**
Cambridge, CB2 1LR (GB)

(74) Representative: **Read, Matthew Charles et al**
Venner Shipley & Co.
20 Little Britain
London EC1A 7DH (GB)

(54) Semiconductor structures

(57) Semiconductor structures and a method of forming semiconductor structures The avalanche breakdown characteristics, such as breakdown voltage and impact ionisation coefficient, of a semiconductor structure can be controlled by controlling the Brillouin-zone-averaged energy bandgap ($<E_c>$) of the material forming the structure. Consequently, the avalanche breakdown characteristics of a device may be tailored independently of the bandgap E_g. The Brillouin-zone-averaged energy bandgap ($<E_c>$) may be controlled by controlling the composition of the semiconductor used or by straining its lattice.

EP 0 757 392 A1

Description

Field of the Invention

The present invention relates to a method of forming a semiconductor structure.

Background

I. General

Pair-production by impact ionisation is one of the most important processes affecting the performance of semiconductor electronic devices. The secondary carriers lead to current multiplication which is used to increase the signal in avalanche photodiodes and phototransistors. However, avalanche breakdown imposes an upper limit on the bias that.can be applied to semiconductor pn junctions, for example in diodes and transistors, which limits the power available from such devices.

In many cases it is desirable to control the likelihood of impact ionisation and avalanche breakdown by means of a suitable choice of semiconductor material, and/or by engineering the electric field profile by means of suitable doping with p- or n-type impurities. Additionally, the conduction band and valence band-structure may be tailored by means of compositional variation (i.e. alloying) or by growth of heterojunctions comprising layered materials of different band-structure. Lattice mis-matched systems may be grown and the resulting strain used to modify the material properties.

The design of semiconductor structures with controlled ionisation or avalanche breakdown properties requires an understanding of the effects of the material properties on the ionisation coefficients. In particular, the energy band-structure is known to have a significant effect on impact ionisation (F. Capasso, *Physics of Avalanche Photodiodes,* Academic, San Diego, 1985). Many attempts have been made to design and engineer structures with artificially enhanced or suppressed ionisation coefficients, but these have been rather unsuccessful and considerable controversy remains concerning the validity of the experimental results.

The failure of these previous attempts has been due to an incorrect understanding of the effect of the band-structure on the ionisation rates and, hence, a use of incorrect or inaccurate prescriptions for the design of devices. As an example, we refer to the prescriptions given in Sze S.M. *Physics of Semiconductor Devices 2nd Edition* (Wiley, 1981) at page 104 for the breakdown voltage V_b in abrupt p-n junctions and linearly graded junctions. These are reproduced below.

Abrupt junction:

$$V_b = 60(E_g/1.1)^{3/2} (N_B/10^{16})^{-3/4} \qquad (1)$$

Linearly graded junction:

$$V_b = 60(E_g/1.1)^{6/5} (a/3x10^{20})^{-2/5} \qquad (2)$$

The parameters E_g, N_B and a are the bandgap the background doping density and the doping gradient respectively. These prescriptions were based on the experimentally measured ionisation coefficients of Ge, Si, GaAs and GaP. A similar prescription has been calculated which applies to p-i-n diodes with a 1μm thick i-layer:

$$V_b = 30(E_g/1.1) \qquad (3)$$

Although, the apparent linear dependence of V_b on the band-gap E_g holds approximately for these materials, it has not been known whether the relation holds for other materials, or how accurate the expression is. Nevertheless, these prescriptions have been widely used and applied to many materials. Furthermore, the basic assumption contained in these formulae, viz. that it is the energy bandgap E_g that primarily determines the ionisation coefficients, is the assumption common to apparently all the previous attempts to control and engineer ionisation coefficients.

Other simple theories of impact ionisation have expressed ionisation coefficients in terms of ionisation threshold energies, phonon energies, and the electron-phonon scattering mean-free path, with the latter two variables treated as parameters which are varied to fit experimental data for the ionisation coefficients [for a detailed review, see F. Capasso, in *Semiconductors and Semimetals* (ed. W.T. Tsang, Academic, New York) **22D** (1986) 1]. Hence these theories have no predictive power in respect of the ionisation characteristics of different materials.

Recently, considerable progress has been made in the first-principles numerical calculation of ionisation coefficients, incorporating the effects of the full bandstructure on the carrier kinematics [Shichijo and Hess, Phys. Rev. B 23, p.4197, 1981], scattering dynamics [M. V. Fischetti and S. E. Laux, Phys. Rev. B**38**, 9721 (1988)] and impact ionisation cross-section [N. Sano and A. Yoshii, Phys. Rev. B**45** (1992) 4171; J. Bude and K. Hess, J. Appl. Phys. **72** (1992) 3554, Y. Kamakura, H. Mizuno, M. Yamaji, M. Morifuji, K. Taniguchi, C. Hamaguchi, T. Kunikiyo, M. Takenaka, J. Appl. Phys. **75** (1994) 3500]. However, few materials have been studied to date. Due to the numerical complexity, no simple relation between the ionisation coefficients or breakdown voltage and energy bandstructure has been expected. Selection of semiconductor materials with desired breakdown properties has therefore been made based on empirical knowledge of the ionisation rates in each material.

Optimisation of semiconductor device performance may impose apparently contradictory requirements on the properties of the constituent materials. For example, high speed operation of a field-effect transistor (FET) requires a material with high transient electron velocity (implying a low electron effective mass and hence narrow bandgap), whereas high power operation requires a high breakdown voltage (previously thought to imply a material with wide bandgap). Similarly, a photodetector for use in the near infra-red wavelength region conventionally requires a material with a narrow direct bandgap, whereas the requirements of low dark current suggest the use of a material with a wide bandgap to reduce both primary generation of dark current and its subsequent multiplication by impact ionisation. Some of these trade-offs have in the past been addressed by using composite structures, in which layers of different material composition perform different functions.

The effect of impact ionisation and breakdown, and hence the ionisation properties desired, are different for different classes of device. Here we summarise design optimisation problems in respect of these properties in Field-Effect Transistors (FETs), bipolar transistors, avalanche photodiodes (APDs) and Impact Ionisation Avalanche Transit Time (IMPATT) diodes.

II. Specific semiconductor device design problems

FETs:

High-speed FET operation requires a material in which carriers have a high effective velocity, and whose transport can be efficiently modulated by the gate. This generally implies a material with a narrow energy bandgap. However, high-power operation requires a high avalanche breakdown voltage which previously has been identified with a wide bandgap.

Known ultra-short gate length FETs have cut-off frequencies well above 100GHz. Many microwave and millimetre-wave applications in optical communications, for example laser drivers and photoreceiver amplifiers, and radio, for example oscillators and low-noise amplifiers, require high-speed devices capable of handling large currents and voltages.

The highest operation frequencies have been obtained in AlInAs/GaInAs high electron mobility transistors (HEMTs). However, the narrow bandgap of InGaAs and the consequent high probability of impact ionisation and Zener tunnelling leads to several problems, including low source-drain breakdown voltage and the presence of "kink" phenomena.

The output power of FETs with GaAs and InGaAs channels is limited by avalanche breakdown. In order to increase the power, heterojunction FETs with doped InP channels have been fabricated. [D. R. Greenberg, J. A. del Alamo & R. Bhat IEEE Trans. Electron Devices, ED 42 1574(1995)]. The smaller ionisation probability of InP, compared with GaAs or InGaAs, leads to increased breakdown voltage and hence voltage swing. A complete absence of ionisation in the channel has been achieved hitherto, with consequently low gate current and low output conductance. However, the cut-off frequency was reduced due to the lower mobility of InP and to the doping in the channel.

To achieve high-frequency and high-power operation of FETs, devices with composite InGaAs/InP channels have been proposed and demonstrated [T. Enoki, K. Arai, A. Kohzen and Y. Ishii, IEEE Trans. Electron Dev. **42**, 1413 (1995)]. Electrons are confined to the high-mobility InGaAs in the low-field regions of the channel, and hence exhibit a high transient velocity. However, when the field is sufficiently high, the carriers undergo real-space transfer into the adjoining InP sub-channel, which exhibits high saturated velocity and high breakdown voltage. Hence the output power is not limited by breakdown in the InGaAs. In this configuration, the scope for independent optimisation of the low-field transport and high-field breakdown is somewhat limited by the requirement that real-space transfer into the InP layer should occur prior to the onset of impact ionisation in the InGaAs channel.

Bipolar transistors:

The output power of bipolar transistors is limited by the breakdown voltage of the base-collector junction, and the operating frequency by the base-collector transit time. As bipolar transistors are reduced in size, high doping is required

in the base and collector to reduce parasitic resistances and base punch-through. The increased field in the base-collector junction leads to impact ionisation and hence base current reversal and "snap-back" phenomena [L. Vendrame, E. Zabotto, A. Dalfabbro, A. Zanini, G. Verzellesi, E. Zanoni, A. Chantre and P. Pavan, IEEE Trans. Electron Dev. 42, 1639 (1995)]. Further, heterojunction bipolar transistors (HBTs) operating in avalanche mode exhibit higher collector-base junction capacitance, lower Early voltage, higher device noise, lower power efficiency, lower cut-off frequency, reduced device switching speed, and degraded maximum frequency of oscillation [J. S. Yuan, Int. J. Electronics **74**, 909 (1993)]. Hence it is necessary to find materials for the collector in which the ionisation probability is reduced, while the saturation velocity remains high or is even increased.

HBTs with wide-bandgap emitters offer improved characteristics such as higher emitter efficiency due to reduced hole injection from the base, decreased base resistance, etc., which lead to improved gain and bandwidth [see S. M. Sze, *Physics of Semiconductor devices,* (Wiley, New York, 1981), Ch. 3]. In conventional AlGaAs/GaAs, AlInAs/GaInAs or InP/GaInAs devices, impact ionisation in the GaAs or GaInAs collector limits the output power. The situation is improved using double heterostructure devices in which the collector is fabricated from a material with lower ionisation coefficients. AlInAs/GaInAs/InP devices with InP collectors exhibited breakdown voltage ≈3 times higher than devices with an InGaAs collector, although with f_t reduced by about 30% [C. W. Farley, J. A. Higgens, W. J. Ho, B.T. McDermott and M. F. Chang, J. Vac. Sci, Technol. B 10, 1023 (1992)]. The energy barrier at the InGaAs/InP interface requires the use of intermediate grading layers to maintain the high-speed operation [H. F. Chau, D. Pavlidis, J. Hu and K. Tomizawa, IEEE Trans. Electron Dev. **40**, 2 (1993)]. More sophisticated designs incorporate an InGaAs/AlInAs chirped superlattice and a doping dipole at the base-collector junction, allowing efficient injection into the InP collector, and exhibit high output power at microwave frequencies [C. Nguyen, T. Y. Liu, M. Chen, H. C. Sun and D. Rensch, IEEE Electron Dev. Lett. 17, 133 (1996)].

GaAs-based HBTs with InGaP collectors exhibit higher breakdown voltage compared to GaAs or AlGaAs collectors [C. R. Abernathy, F. Ren, P. W. Wisk, S. J. Pearton and R. Esagui, Appl. Phys. Lett. **61**, 1092 (1992)]. Thin highly-doped GaAs or GaInP layers in the collector were required to maintain the current saturation characteristics [J. I. Song, C. Caneau, W. P. Hong and K. B. Chough, Electron. Lett. **29**, 1881 (1993)].

APDs:

Impact ionisation is the direct cause of avalanche multiplication and hence photocurrent gain in APDs. Hence, sufficiently high ionisation coefficients are required so that avalanche breakdown occurs at sufficiently low fields (e.g. before breakdown due to Zener tunnelling). The penalty for large photocurrent multiplication is excess noise due to the stochastic nature of the ionisation process. The carrier avalanche leads to a finite build-up time of the photocurrent response, and to a sensitive dependence on the applied bias. The noise factor, build-up time and gain stability are all optimised when there is a large difference between the ionisation coefficients of electrons (α) and holes (β). For a full discussion, see Capasso [*ibid*]. Low-noise operation also requires a low dark current (e.g. due to band-to-band tunnelling).

The selection of materials for APDs is constrained by the desired optical wavelength for detection, which is a function of bandgap. Unfortunately, the common direct band-gap III-V materials such as GaAs, InP and InGaAs have equal (within a factor ≈2) electron and hole ionisation rates, and hence high excess noise. Narrow bandgap materials such as InGaAs, which are sensitive in the technologically-important near-infrared region, suffer from large leakage currents at high fields due to band-to-band tunnelling. Only silicon exhibits unambiguously a large difference between electron and hole ionisation rates, but its absorption coefficient at visible/infrared wavelengths is small due to its indirect bandgap.

SAM APDs

In the Separate Absorption and Multiplication (SAM) APD, one layer such as InGaAs, absorbs incoming light, while carrier multiplication occurs in an adjacent high-field layer composed of a material such as InP [O. K. Kim, S. R. Forrest, W. A. Bonner and R. G Smith, Appl. Phys. Lett. **39**, 402 (1981)]. Careful control of the doping is required so that the field at the heterointerface between the layers is sufficient to ensure collection of the carriers but not high enough to allow tunnelling in the InGaAs. The abrupt heterointerface causes pile-up of photogenerated holes; this deleterious effect can be ameliorated by compositional grading of the heterointerface. SAM APD's with a Si multiplication region and SiGe superlattice region absorbing light at 1.3 μm have also been demonstrated. The low absorption coefficient necessitated a waveguide geometry to increase the absorption length without drastically increasing the transit time [H. Temkin, A. Anredsyan, N. A. Olsson, T. P. Pearsall & J. C. Bean, Appl. Phys. Lett. 49, 809 (1996)].

Bandgap engine ring for enhanced ionisation rates in APDs

Since no material has been found which exhibits large multiplication, low dark current, high absorption coefficient over a range of optical wavelengths, and significantly differing electron and hole ionisation coefficients, many attempts have been made to design and engineer APDs with modified (usually enhanced) ionisation rates. The assumption common to these attempts is that the energy bandgap E_g primarily determines the ionisation coefficients. Control is attempted by varying either the bandgap itself, or the bandstructure (e.g. effective mass, spin-orbit splitting, etc.) in a restricted region of the Brillouin zone such as the region immediately in the vicinity of the local conduction-band minimum defining the band-gap, or the heterojunction discontinuities appropriate to a restricted region of the Brillouin zone such as the region in the vicinity of the bandgap. Previously-investigated structures include the graded-gap APD, multiple quantum well or superlattice APD and the staircase photomultiplier [for a review, see F. Capasso, ibid].

Graded-gap APD:

Kroemer [H. Kroemer, RCA Rev. **18**, 332 (1957)] showed that electrons and holes in a compositionally-graded semiconductor experience quasi-electric fields whose force pushes the carriers in the same direction towards regions of lower bandgap. Capasso [F. Capasso, US Pat. 4383269 (1983)] described a p^+-i-n^+ APD in which the i-region consists of a graded-gap semiconductor. An applied electric field accelerates the electrons and holes in opposite directions. Hence electrons and holes experience different electric fields, and therefore different ionisation coefficients. Experiments on graded-gap AlGaAs structures suggested some enhancement of (α/β) compared to GaAs [F. Capasso, W. T. Tsang, A. L. Hutchinson, and P. W. Foy, Inst. Phys. Conf. Ser 63, 473 (1992)]. Ionisation occurs at lower fields in the narrow-gap regions of the graded-gap APD than in the wide-gap regions, leading to more gradual breakdown and hence more stable gain.

Multiple quantum well APD:

Chin et al. [R. Chin, N. Holonyak and G. E. Stillman, Electron. Lett. **16**, 467 (1980)] predicted that ionisation rates could be enhanced in semiconductor multiple quantum wells (MQWs) or superlattices. Carriers crossing a heterojunction from a wide-gap to a narrow-gap material increase their kinetic energy by an amount equal to the potential discontinuity. The high energy tail of the carrier distribution, and hence the number of carriers at energies where ionisation occurs, is increased. At a heterojunction in which the potential discontinuities for electrons and holes are significantly different, one carrier type can be selectively enhanced leading to an increase in the ionisation coefficient ratio. Hence the noise, response time and gain stability can be improved. The spatial localisation of the ionisation event within a short distance of the heterojunctions also further decreases the multiplication noise.

Capasso et al. [F. Capasso, W. T. Tsang, A. L. Hutchinson and G. F. Williams, Appl. Phys. Lett. **40**, 38 (1982)] reported $(\alpha/\beta) \approx 8$ in 500Å AlGaAs / 500Å GaAs MQW APD (Figure 4c), compared to $(\alpha/\beta) \approx 2$ in bulk GaAs. It should be noted that these measurements, and the measurements of enhanced (α/β) in graded-gap APDs mentioned above, were performed before the definitive experimental study of ionisation coefficients in GaAs by Bulman et al.[G. E. Bulman, V. M. Robbins, K. F. Brennan, K. Hess and G. E. Stillman, IEEE Electron. Dev. Lett. **EDL-4**, 181 (1983)], which pointed out the role of electroabsorption of recombination radiation in contaminating measurements of ionisation coefficients. More recent measurements [P. Aristin, A. Torabi, A. K. Garrison, H. M. Harris and C. J. Summers, Inst. Phys. Conf. Ser. **120**, 523 (1991); A. Salokatve, M. Toivonen and M. Hovinen, Electron. Lett. **28**, 416 (1992)] have found no difference between ionisation coefficients in the GaAs wells of the MQW, and bulk GaAs. In contrast, InAlAs/InGaAs superlattice APDs have exhibited clear evidence of (α/β) enhancement, and exhibit gain-bandwidth products > 100GHz [K. Taguchi, K. Makita, I. Watanabe, M. Tsuji and S. Suguo, Optoelectronics - Devices and Technol. 10, 97 (1995)].

Staircase photomultiplier:

The performance of the MQW APD is expected to be optimised for electron multiplication when the valence-band discontinuity is minimised, and the conduction-band is larger than the bandgap ($\Delta E_c > E_g$). However in such a case, compositional grading of the well-barrier exit heterojunction is required to prevent electron trapping in the quantum wells. These considerations led to the proposal of the staircase APD [G.F. Williams, F. Capasso and W. T. Tsang, IEEE Electron. Dev. Lett. **EDL-3**, 71 (1982)]. Due to the single carrier-type multiplication and the spatial localisation of the impact ionisation, the device acts as a solid state analogue of the photomultiplier. Material systems which have been identified as satisfying (or almost satisfying) the condition $\Delta E_c > E_g$ include $AlAs_{0.03}Sb_{0.97}$/GaSb and HgTe/CdTe [F. Capasso, in *Semiconductors and Semimetals* (ed. W.T. Tsang, Academic, New York) **22D** (1986) 1].

Staircase APD's which incorporate multiple graded layers but do not satisfy the condition $\Delta E_c > E_g$, have been fabricated using GaAs/$Al_{0.45}Ga_{0.55}As$ with doping dipoles at the heterojunction interfaces to increase the effective band

offset [M. Toivonen, A. Salokatve, M. Hovinen, AND M. Pessa, Electron. Lett. **28**, 32 (1992)], and also using InAlGaAs with ΔE_c up to 0.5eV [M. Tsuji, K. Makita, I. Watanabe and K. Taguchi, Jap. J. Appl. Phys. **34**, L1048 (1995)]. In both cases, (α/β) was increased from ≈2 in the bulk materials to ≈ 5. Staircase APDS fabricated from amorphous hydrogenated SiC/Si [K. Sawada, S. Akata, T. Takeuchi and T. Ando, Appl. Phys. Lett. 68, 1835 (1996)], and amorphous hydrogenated SiC/SiGe multilayer APDs in which the conduction-band discontinuity exceeds the bandgap [S. Sugawa, A. Kozuka, T. Atoji, H. Tokunaga, H. Shimizu and K. Ohmi, Jap. J. Appl. Phys. **35**, 1014 (1996)], have been reported.

IMPATTs:

IMPATT diodes depend on the time delay caused by avalanche build-up of secondary carriers and their subsequent drift, which can yield a negative resistance in the diode characteristic at microwave frequencies. Such devices offer the highest power sources of microwave and millimeter-wave radiation [for detailed discussion and references, see S. M. Sze, *Physics of Semiconductor devices,* (Wiley, New York, 1981), Ch. 10]. The power-frequency limit of the IMPATT diode depends on the saturated carrier velocity v_s and the avalanche breakdown voltage V_b. The frequency is also limited by the avalanche build-up time and hence depends on the ratio of electron to hole ionisation coefficients. Output efficiency is maximised when a high carrier velocity can be maintained at low fields. In contrast to the case for APDs, the minimum noise in an IMPATT diode is achieved when electron and hole coefficients are similar in magnitude, so that GaAs $(\alpha/\beta \approx 2)$ offers lower noise than Si $(\alpha/\beta \approx 10)$ [Sze, *ibid*].

Various junction structures are utilised, including Read, double-drift and Misawa diodes. With a few exceptions, IMPATT diodes have been restricted to Si, GaAs or InP, although IMPATT devices using different materials for the avalanche and drift regions have been reported. Higher power and lower noise were claimed for AlGaAs/GaAs heterojunction IMPATTs [J. C. DeJaeger, R. Kozlowski and G. Salmer, IEEE. Trans. Electron. Dev. 30, 790 (1983); Electron. Lett. **20**, 803 (1984); M.J. Bailey, Microwave J. **36**, 76 (1993); IEEE Trans. Electron. Dev. **39**, 1829 (1992); M. J. Kearney, N. R. Couch, R. S. Smith and I. S. Stephens, J. Appl. Phys. 71, 4612 (1992)]. However other studies conclude there is little advantage for this material system [M. J. Kearney, N. R. Couch, J. Stephens and R. S. Smith, Semicond. Sci. Technol. 8, 560 (1993)]. Improved performance was also predicted for GaAs/InGaAs/GaAs IMPATTs [G. N. Dash and S. P. Pati, Appl. Phys. A, 58,211 (1994)].

IMPATTs with superlattice avalanche regions have been proposed [C. C. Meng and H. R. Fetterman, Solid-State Electron. 36, 435 (1993); K.K. Chandramojhan, R. U. Khan and B. B. Pal, J. Inst. Electr. Telecom. Eng. **40**, 261 (1994)], and some performance enhancement claimed [C. C. Meng, S. W. Siao, H. R. Fetterman, D. C. Streit, T. R. Block and Y. Saito, Micro. and Opt. Tech. Lett. **10**, 4 (1995)].

Hence, in summary, materials for FET channels, HBT collectors, and IMPATT devices require high breakdown voltage and high saturated carrier velocity. APDs and IMPATTs require control of the ratio of the electron to hole ionisation coefficients (α/β). Thus, from the foregoing, it will be seen that there are a number of different conflicting deisgn requirements for the impact ionisation and breakdown characteristics for semiconductor devices, which can only partially be resolved by conventional design techniques. These problems and constraints may at least in part be ameliorated by the present invention.

Summary of the Invention

According to the present invention, there is provided a method of forming a semiconductor structure comprising forming a semiconductor structure such that the Brillouin-zone-averaged energy bandgap ($< E_c >$) of at least a portion of the structure is controlled on the basis of a desired avalanche breakdown characteristic therefor. The present invention applies particularly to materials having relatively large bandgaps (E_g> 1eV), including (but not limited to) GaAs, InP, GaP, AlAs, AlSb and AlP.

It has been found that for most practical purposes the following relationship holds:

$$\frac{1}{8}(E_\Gamma + 4.E_L + 3.E_X) = <E_c> \qquad (4)$$

where E_r is the conduction band-edge energy at the Γ symmetry point of the Brillouin zone, measured relative to the valence band maximum at Γ, E_x is the conduction band-edge energy at the X symmetry point of the Brillouin zone, measured relative to the valence band maximum at Γ, E_L is the conduction band-edge energy at the L symmetry point of the Brillouin zone, measured relative to the valence band maximum at Γ.

The portion of the structure may be formed according to the invention by:

(a) selecting from "known" materials, such GaAs, InP, on the basis of their $< E_c >$ values which are fixed;

(b) forming an alloy with a predetermined value of $< E_c >$ and if required also a predetermined value of E_g or lattice

constant;

(c) forming of a strained layer or strained layer superlattice such that a predetermined value for $< E_c >$ is established by the strain;

(d) forming a compositionally graded region in which the variation of $< E_c >$ with position (x) leads to an additional effective field $d < E_c > /dx$, to enhance or suppress ionisation/breakdown depending on whether it is aligned parallel or anti-parallel to the applied electric field;

(e) forming a superlattice pseudoalloy; or

(f) forming a multilayer heterojunction system to create a superlattice or multiple quantum well, in which ionisation may be enhanced by means of the energy gained at the heterojunction in crossing from a region of high $< E_c >$ to a region of low $< E_c >$.

A device according to the invention may be formed using any combination of the methods (a) to (f) listed above.

Forming a compositionally graded region allows the possibility of engineering both $< E_c >$ and E_g such that either E_g is constant and $< E_c >$ is graded or $< E_c >$ is constant and E_g is graded.

It is known that strain in the lattice of a semiconductor also affects the band-structure. Thus, the avalanche breakdown characteristics can be tailored by growing mis-matched lattice layer in the formation of a semiconductor structure. The control of E_x and E_L may also be achieved by varying the composition of the semiconductor material. Consequently, by the use of suitable lattice strains and material compositions, $< E_c >$ and E_g can both be tailored to the requirement of a particular device. Thus, it can be seen that the avalanche breakdown voltage or the ionisation coefficient for a junction can be varied somewhat independently of the energy bandgap E_g.

Grading $< E_c >$ or forming the structure with discontinuities in $< E_c >$ enables X and L electrons to be accelerated as well as the Γ electrons.

Conveniently, the Brillouin-zone-averaged energy bandgap of a p-i-n diode can be selected according to the following relationship:

$$<E_c> = \frac{(V_b + m)}{n} \qquad (5)$$

where V_b is a predetermined breakdown voltage, and m and n constants. In the case of a p-i-n diode having a 1μm wide i region, m is approximately 45.8 and n is approximately 46.3. Other relationships between breakdown voltage V_b and $< E_c >$ can be calculated for other doping profiles, e.g. abrupt or graded.

The present invention also provides a semiconductor device having a region wherein the energy gap is substantially constant and the Brillouin-zone-averaged energy bandgap varies spatially and a semiconductor device having a region wherein the energy gap varies spatially and the Brillouin-zone-averaged energy bandgap is substantially constant.

Brief Description of the Drawings

Embodiments of the present invention will now be described, by way of example, with reference to the accompanying drawings, in which:

Figure 1(a) is a graph of the band gap energy E_g as a function of alloy composition in $Al_xGa_{1-x}As$ and $(Al_xGa_{1-x})_{0.52}In_{0.48}P$, based on the data of Table I;

Figure 1(b) is a graph of the measured breakdown voltage V_b as a function of composition (x);

Figure 2(a) is a diagram of the energy gaps in a semiconductor, illustrating the gap E_g and direct optical transitions E_0, E_1 and E_2 in Ge;

Figure 2(b) is a diagram of the density of energy states, showing average gaps $<E_G>$ and $<E_c>$;

Figure 3(a) is a graph of band energy E_B for the valance band (V_B), conduction band (C_B) and midgap (DME) energies at the Baldereshi point (LMTO calculation) plotted against the values of the Penn gap;

Figure 3(b) is a graph of conduction band energy E_c and direct bandgap E_g at the Chadi-Cohen special point E_{CC}, as compared with the Kleinmann-Phillips average E_{KP} (empirical pseudopotential calculation);

Figure 4(a) is a graph of the theoretical indirect energy gaps calculated for a range of semiconductors compared with their experimental values;

Figure 4(b) corresponds to Figure 4(a) but for direct energy gaps;

Figure 5(a) is a graph of V_b as a function of bandgap E_g;

Figure 5(b) is a corresponding graph of the breakdown voltage V_b as function of the average energy $< E_c >$;

Figure 6(a) is a graph illustrating the dependence of V_b on average energy gaps $< E_c >$ for indirect and $< E_G >$ for direct transition in k space;

Figure 6(b) is a graph of the breakdown voltage V_b as a function of Eg for narrow bandgap materials and as a function of $< E_c >$ for wide bandgaps materials;

Figure 7(a) is a graph of V_b for Al_xGa_{1-x} and $(Al_xGa_{1-x})_{0.52}In_{0.48}P$ as a function of direct bandgap E_Γ for room temperature measurements;

Figure 7(b) corresponds to Figure 7(a), but as a function of $< E_c >$;

Figure 8 (a) is an energy diagram illustrating threshold energies for electron-initiated impacted ionisation processes along the (100) axis in respect of the final electron states in the Γ valley;

Figure 8(b) is a graph corresponding to Figure 7(a) for final electron states in the X valley;

Figure 9(a) is an energy diagram of the barriers associated with pair-production for final states in the Γ, X and L minima;

Figure 9(b) illustrates the degeneracy of conduction-band values in a tetrahedrally-coordinated semiconductor;

Figure 10 illustrates how energy levels may be engineered in accordance with the invention, wherein in Figure 10 (a) material has a relatively narrow bandgap E_g and a relatively small value of $< E_c >$, in Figure 10(b) the material has a relatively narrow bandgap E_g and a relatively large $< E_c >$, and in Figure 10(c) a relative wide bandgap E_g and a relatively large $< E_c >$;

Figure 11(a) illustrates the minimum energy gap E_g and the corresponding value of $< E_c >$ for a number of III-V compounds;

Figure 11(b) corresponds to the diagram of Figure 11(a), for a number of group IV elements and III-VI compounds;

Figure 12 illustrates various bandedge profiles for compositionally graded structures possible according to the present invention;

Figure 13(a) illustrates the band structure of a pseudoalloy with layer thicknesses ≈ 1nm;

Figure 13(b) illustrates the band structure of a pseudoalloy with layer thicknesses 1 ≈ 10nm;

Figure 13(c) shows the band structure of a pseudoalloy with layer thickness > 10nm;

Figure 14(a)-(d) illustrates the band structures of quantum well structured with different values of $< E_c >$ and E_g selectible quasi-independently for separate control of light absorption and breakdown;

Figure 15 is a cross-sectional diagram of a first embodiment of FET manufactured in accordance with the invention;

Figure 16 corresponds to Figure 13, for a second embodiment of FET manufactured in accordance with the invention;

Figure 17 is a corresponding cross-sectional view of a third embodiment of FET manufactured in accordance with the invention;

Figure 18 illustrates a fourth embodiment of FET manufactured in accordance with the invention;

Figure 19 illustrates a fifth embodiment of FET manufactured in accordance with the invention;

Figure 20 illustrates a sixth embodiment of FET in accordance with the invention;

Figure 21 is a schematic cross sectional view of a bipolar transistor;

Figure 22(a) and (b) illustrate energy band diagrams for prior art single and double heterojunction bipolar transistors;

Figures 22(c) and (d) illustrate corresponding energy band diagrams for single and double heterojunction bipolar transistors in accordance with the invention;

Figure 23(a) and (b) illustrate schematically in cross section a first example of materials used in prior art bipolar transistors with single and double heterojunctions respectively;

Figure 23(c) and (d) illustrate corresponding structures, with material systems selected in accordance with the invention;

Figure 24 (a) and (b) illustrate schematic cross sections of the base-emitter-collector of prior arts single and double heterojunctions bipolar transistors;

Figure 24(c) and (d) illustrate corresponding arrangements in which the materials have been selected in accordance with the method of the invention;

Figure 25 is a schematic cross sectional view of a APD;

Figures 26 to 28 are energy band diagrams of APDs according to the prior art;

Figure 29 is a corresponding energy band diagram for an APD in accordance with the invention;

Figure 30 is a schematic cross sectional view of a quantum well APD in accordance with the invention that utilises a strained superlattice;

Figure 31 is an energy band diagram for the device shown in Figure 30;

Figure 32 is a schematic cross sectional view of a SAM-APD in accordance with the invention;

Figure 33 is an energy band diagram of the SAM-APD shown in Figure 32;

Figure 34(a) illustrates Zener tunneling in the quantum well structure shown in Figure 32;

Figure 34(b) illustrates how the quantum barriers can be made higher in the device of Figure 32 in order to minimise Zener tunneling;

Figure 34(c) illustrates spatial modulation in the layer thicknesses in order to allow charge carriers to pass out of

the wells;

Figure 35(a)-(d) are schematic cross sectional views of different IMPATT devices fabricated according to the method of the invention; and

Figures 36(a)-(d) are corresponding more detailed views of the drift avalanche regions of the devices shown in Figures 35(a)-(d); and

Figure 37 illustrates another diode in accordance with the invention.

Detailed Description

I. Analysis

In investigating the dependence of impact ionisation on bandstructure for a range of materials, we encounter problems in determining both V_b and the bandgaps. Ionisation coefficients for many materials are not well established; with significant discrepancies amongst the published values. For direct, narrow-bandgap materials ($E_g \leq 0.8eV$), interband tunnelling can cause breakdown at fields lower than that required for impact ionisation. In wide bandgap materials, localised premature breakdown at "microplasmas" or edges of the device can occur. In any case, extraction of accurate ionisation coefficients from measurements on a semiconductor device depend upon a reliable determination of the electric field profile within the device. We will utilise recent work by Davide et al [J.P.R. David, M. Hopkinson and M. A. Pate, Electron. Lett. 30, 909 (1994)], in which V_b was directly measured in 1μm p-i-n diodes fabricated in two alloy systems: $Al_xGa_{1-x}As$ and $(Al_xGa_{1-x})_{0.52}In_{0.48}P$. To account for variations in the doping levels and i-region width, the internal field distribution of the devices was measured, and the breakdown voltages were normalised to that for a GaAs device with the same structure. The results are shown in Table I. Both alloy systems are lattice-matched to GaAs, and exhibit a direct-indirect bandgap transition within the range of composition studied.

The bandstructure parameters such as energies at symmetry points in the Brillouin zone, are not well known in all cases. However, the room-temperature conduction-band energies have been measured experimentally for $Al_xGa_{1-x}As$ and $(Al_xGa_{1-x})_{0.52}In_{0.48}P$, and are shown in Table I. The results for $Al_xGa_{1-x}As$ have been summarised by Adachi [S. Adachi, EMIS Data Review 7, (INSPEC, 1993)]. Recently, Prins et al [A.D. Prins, J.L. Sly, A.T. Meney, D.J. Dunstan, E.P. O'Reilly and A.R. Adams, Proc. 22nd Int. Conf. Phys. Semicond., 727 (1995)], have measured E_Γ and E_x for $(Al_xGa_{1-x})_{0.52}In_{0.48}P$. Values for E_L have been obtained by interpolating between the constituent binary alloys.

We first investigate the dependence of V_b on E_g. Figure 1(a) shows its composition dependence in the two alloy systems. The arrows mark the transition from direct to indirect bandgap regimes. However, as shown by David et al [J.P.R. David, M. Hopkinson and M.A. Pate, Electron. Lett. **30**, 909 (1994)] and reproduced in Figure 1(b), V_b increases linearly with the composition x in both $Al_xGa_{1-x}As$ and $(Al_xGa_{1-x})_{0.52}In_{0.48}P$. The absence of deviation from linearity at the direct-indirect transition immediately demonstrates that E_g is not the important parameter in determining V_b: Furthermore, it is seen that for alloys with the same value of E_g such as $Al_{0.35}Ga_{0.65}As$ and $Ga_{0.52}In_{0.48}P$, V_b is ≈ 20% higher in the latter material. Hence the dependence of V_b on the bandstructure involves some other parameter than E_g.

Average energy gaps and special k-points

The value of the energy gap is dependent on both the magnitude and direction of the wavevector **k**. Figure 2(a) shows the energy bandstructure of Ge in the first Brillouin zone of momentum space. The smallest value of the energy gap (E_g) determines the threshold for interband optical absorption and many aspects of electronic transport at low fields, while the direct gaps E_0, E_1 and E_2 dominate the optical spectra. For wide-bandgap semiconductors (as defined hereinbefore), carriers at the high energies required for impact ionisation undergo rapid scattering with phonons, randomising the momentum. Hence we might expect that ionisation threshold energies are associated not with E_g but instead with some average value of the energy gap. The average direct gap between valence and conduction bands ($< E_G >$ in Figure 2(b)), also known as the bond energy gap or Penn gap, arises from the gap between bonding and antibonding energy levels. A single-isotropic-gap Penn model is able to reproduce many of the features of the bond strength and dielectric response of semiconductors [J.C. Phillips, "Bonds and bands in semiconductors", Academic Press, New York, 1973].

During pair-creation by impact ionisation, the initiating carrier exchanges momentum with a valence electron, i.e. transitions are indirect in k-space. Semiconductors with the zincblende crystal structure are characterised by having a single valence-band maximum at Γ and local conduction-band minima at Γ, X and L. We can therefore also consider an average indirect bandgap between the valence-band maximum and the average conduction band energy, shown as $< E_c >$ in Fig 2(b).

The average energy gaps $< E_G >$ and $< E_c >$ may be calculated by integration over the entire Brillouin zone, which is an intensive calculation. However, good approximations may be achieved by considering a small number of "special points" in the Brillouin zone. The best single-point representation of the Brillouin zone is known the Baldereschi mean-

value point [A. Baldereschi, Phys. Rev. B7, 5212 (1973)].

$$(E) = E_B = E(0.6223, 0.2963, 0) \qquad (6)$$

where the k-coordinates are in units of $(2\pi/a_0)$. Cardona and Christense [M. Cardona and N.E. Christensen, Phys. Rev. B. 35, 6182 (1987)] have shown that the Penn gap is associated with the valence-conduction band separation at the Baldereschi special point. Figure 3(a) shows their calculated valence- and conduction-band energies at the Baldereshi point (E_B) plotted against the values of the Penn gap given by Phillips (E_G) for group IV, III-V and II-VI semiconductors, after correcting for shifts of the energy bandgaps associated with the local density functional calculation. The dielectric midgap energy (DME) is found to be a useful parameter in studies of both the electron-phonon interaction and bandgap discontinuities at heterojunctions, see Cardona et al, ***supra.***

A more accurate special-point representation is that of Chadi and Cohen [D. J. Chadi and M. L. Cohen, Phys. Rev. **B8** (1973) 5747].

$$(E) = E_{CC} = \frac{3}{4} E(0.75, 0.25, 0.25) + \frac{1}{4} E(0.25, 0.25, 0.25) \qquad (7)$$

However, for our purposes the most convenient representation is due to Kleinman and Phillips [L. Kleinman and J. C. Phillips, Phys. Rev. 116 (1959) 880].

$$(E) \approx E_{KP} = \frac{1}{8} [E(0,0,0) + 3 \cdot E(1,0,0) + 4 \cdot E(0.5,0.5,0.5)] = \frac{1}{8} [E_\Gamma + 3 \cdot E_X + 4 \cdot E_L] \qquad (8)$$

Although slightly less accurate than the Chadi-Cohen representation, it has the advantage that the special points are at the Γ, X and L symmetry points of the Brillouin zone, for which experimental data for the energies is directly available. We have verified the relationship between E_{CC} and E_{KP} by performing an empirical pseudopotential calculation for 14 cubic semiconductors using the parameters of Cohen and Bergstrasse [M. Cohen and T. K. Bergstrasser, Phys. Rev. 141, 789 (1965)]. Figure 3b compares the $< E_c >$ and $< E_G >$, calculated using the special point of Kleinman-Phillips and Chadi-Cohen. As expected, the two methods yield energies which are related by straight line of unity slope.

Determination of reliable bandstructure data

Study of the dependence of avalanche breakdown and average energies for a wide range of materials demands a reliable and consistent set of bandstructure data. The most accurate semiconductor bandstructures have been determined from empirical variation of the crystal pseudopotential to fit known critical point energies,[J. R. Chelikowsky and M. L. Cohen, Phys. Rev. **B14**, 556 (1986).] but are only as reliable as the experimental energies. For several materials which have been less thoroughly studied, there is insufficient experimental data to allow determination of the empirical pseudopotential. Recently, ab-initio theoretical calculations of the bandstructures have been performed, which predict energies in good agreement with experiments. Such calculations provide an invaluable guide to the interpretation of experimental bandstructure measurements and to the properties of materials for which little experimental information is available.

Louie and coworkers have performed model dielectric quasiparticle calculations for a large number of semiconductor compounds with the diamond or zincblende crystal structure; C, Si and Ge; BN, BP and BAs; AlN and GaN; binary III-V compounds containing Al, Ca, In, P, As and Sb, and some ternary alloys; and binary II-VI compounds containing Zn, Cs, S, Se and Te. For further details reference is directed to M .S. Hybersten and S. G. Louie, Phys. Rev. **B34**, 5390 (1986); M. P. Surh, S. G. Louie and M. L. Cohen, Phys. Rev. **B43**, 9126 (1991); A.Rubio, J.L. Corkill, M. L. Cohen, E. L. Shirley and S. G. Louie, Phys. Rev. **B48**, 11810 (1993); X. Zhu and S. G. Louie, Phys. Rev. **B43**, 14142 (1991) and O. Zakharov, A. Rubio, M.L. Cohen and S. G. Louie, Phys. Rev. **B50**, 10780 (1994). The energy gaps are shown in Table II (indirect gaps) and Table III (direct gaps), for absolute zero temperature. Figure 4 shows a comparison of the theoretical energies with experimental values, as collated by Louie and coworkers. Figure 4(a) shows the data for indirect energy gaps and Figure 4(b) shows data for direct gaps. The arrows indicate significant discrepancies probably associated with the experiments. A linear fit to remaining points (dashed line) accounts for systematic errors in the calculation. Significant discrepancies occur for BP, for which little experimental data is available, and for Al-containing compounds, in which surface oxidation can strongly influence the value of the bandgaps measured by optical techniques. The difference between theory and experiment for the remaining points is less than 0.3eV(typically 0.1eV). A linear fit removes a small systematic error associated with the theoretical calculation, and improves the agreement for the bandgap of narrow-gap materials such as InAs and InSb (see Tables II and III). In order to obtain

the most reliable set of bandgaps and average energies, the experimental values have been used where the agreement between experiment and theory is good; elsewhere the theoretical values are taken. The remaining errors are sufficiently small to allow examination of the scaling of the avalanche breakdown voltage with the average energy gaps.

Universal dependence of V_b on $< E_c >$

Having determined a reliable and consistent set of bandstructure parameters, and having established that the Kleinman-Phillips method represents a suitable calculation of average energies, we can now examine the dependence of avalanche breakdown on the band structure. Table IV shows the values of E_g, E_Γ, $< E_c >$ and $< E_G >$ for semiconductors for which experimental measurements of the ionisation coefficients have been performed: Si, Ge, GaP, InP, GaAs, $Ga_{0.47}In_{0.53}As$, $Al_{0.48}In_{0.52}As$, $Al_xGa_{1-x}As_ySb_{1-y}$, $Al_xGa_{1-x}As$ and $(Al_xGa_{1-x})_{0.52}In_{0.48}P$. The energy gaps for the alloys were obtained by linear interpolation between the constituent binary compounds (i.e. no account of compositional or positional disorder was made) The avalanche breakdown voltage V_b was calculated for a 1μm p-i-n diode, or was measured directly in the case of $Al_xGa_{1-x}As$ and $(Al_xGa_{1-x})_{0.52}In_{0.48}P$ [J.P.R. David, M. Hopkinson and M. A. Pate, Electron. Lett. 30, 909 (1994)].

Figure 5(a) shows the dependence of V_b on E_g (E_Γ in the case of $Al_xGa_{1-x}As$ and $(Al_xGa_{1-x})_{0.52}In_{0.48}P$). Although a general trend of V_b increasing with E_g is followed, deviations of up to 30% are observed compared to equation (3). Hence the formula of Sze and Gibbons (equations (1) to (3) do not provide a reliable estimate of V_b. In marked contrast, as shown in Figure 5(b) there is a simple linear relationship between V_b and the average conduction-band energy $< E_c >$ which is obeyed by all the wide bandgap ($E_g >$ leV, $< E_c > > 1.5$eV) semiconductors with the possible exception of GaP. The relation is described by:

$$V_b = 45.8 * (< E_c > - 1.01) \qquad (9)$$

or

$$\frac{V_b}{V_b(GaAs)} = 2.41 \frac{< E_c >}{< E_c > (GaAs)} - 1.37 \qquad (10)$$

where the parameters have been normalised to those of GaAs. Deviations from linearity are well within the uncertainties associated with $< E_c >$ and V_b. The apparent discrepancy for GaP may relate to an experimental artefact; we might expect a breakdown voltage of ≈78V rather than the (1965) reported value of ≈ 61V, based on extrapolation of the values for InP and $Ga_{0.52}In_{0.48}P$.

Figure 6(a) compares the dependence of V_b on $< E_c >$ and $< E_G >$. Although there is slightly more spread in the V_b ($< E_G >$) data, it cannot be conclusively decided whether V_b depends primarily on $< E_c >$ or $< E_G >$, or indeed some combination due to the presence of both direct and in direct transitions of k-space. $< E_c >$ and $< E_G >$ are closely related due to the similarity of the valence bands for zincblende semiconductors. Hence this work reveals an unexpected direct relationship between V_b and the Penn gap $< E_G >$.

As shown in Figure 6(b), narrow gap materials, including Ge, GaSb, and presumably InAs and InSb, do not obey the scaling relation (9). Indeed it is clear that the relation must fail since it predicts $V_b \leq 0$ for $< E_c > \leq 1.0$eV. It is known that impact ionisation in narrow-gap materials such as InAs occurs predominantly in the Γ valley; the field required for avalanche breakdown is lower than that required for intervalley transfer since the bandgap E_g is small compared to the intervalley separations. Hence a description of the effective ionisation threshold energy in terms of an average conduction band energy is no longer appropriate. $Ga_{0.47}In_{0.53}As$ represents a material which is close to the boundary between narrow and wide bandgap materials. At low fields, ionisation occurs predominantly in the Γ valley, whilst at high fields, ionisation occurs throughout the Brillouin zone. This behaviour is the origin of the different field-dependence at low- and high-fields, observed in the theoretically-calculated [J. Bude and K. Hess, J. Appl. Phys. **72** (1992) 3554] and experimentally-measured [C. Canali, C. Forzan, A. Neviani, L. Vendrame E. Zanoni, R. A. Hamm, R.J.Malik, F. Capasso and S. Chanrasekhar, Appl. Phys. Lett. **66**, 1095 (1995)] ionisation coefficient in $Ga_{0.47}In_{0.53}As$.

Further evidence for the relationship of equation (9) can be obtained by comparison of the measured room-temperature breakdown voltages and the measured room-temperature energy gaps (see Table I). Figures 7(a) and (b) show V_b plotted against E_Γ and $< E_c >$ respectively. The dependence on $< E_c >$ rather than E_g is clearly confirmed.

As an example of the use of our prescription, we compare the breakdown voltage in GaAs and InP. Despite having a smaller bandgap, the breakdown voltage in InP is ≈ 30% higher than in GaAs, as a result of the larger value of $< E_c >$. Furthermore, we can predict the breakdown voltage in materials such as AlAs, AlSb and AlP etc., for which no results have been reported to our knowledge as shown in Table V. Very high breakdown voltages (> 100V) are expected

in materials such as (Al, Ga) N, B(P, As) and (Zn, Cd) (S, Se) with $< E_c >$ as high as 3eV or more.

Some comment on the Sze and Gibbons formulae (1) - (3) can be made. These expressions were obtained by fitting to experimental data for Ge, GaAs, Si and GaP. GaAs and Si have rather similar bandgaps and breakdown voltages. According to our analysis, Ge does not fit the trend obeyed by wide gap materials, and the data for GaP is erroneous. Hence the Sze and Gibbons expressions appear to be without reliable basis.

Physical interpretation

We interpret the existence of equation (9) as evidence for the distribution between conduction-band minima of final electron states of the pair-production process. Figure 7 shows the calculated thresholds for electron-initiated processes with all wavevectors directed along (100). For a similar initial state (when umklapped into the first Brillouin zone), the process produces final states of different symmetry, either in the Γ or the X valleys. Since the excess energy of the final electron states (relative to the minimum potential energy of the appropriate valley) is small, the final states have well-defined symmetry and are described by effective-mass properties of the minimum. Hence the effective energy barrier for impact ionisation can be expected to scale with the bandgap energy from the valence band maximum to the Γ, X or L conduction band minima as shown in Figure 8. Due to the high scattering rates experienced by carriers which initiate impact ionisation, their momentum is randomised and hence initial states corresponding to pair-production with final electron states in the different conduction-band minima are widely available. If the intervalley separations are small compared to the bandgap, the distribution of final electron states between Γ, X and L valleys is determined primarily by the density of states, which is given to lowest order by the degeneracy of the valleys, as illustrated in Figure 9. The energy barrier for pair-production is thus largely determined by $< E_C >$.

Conclusions

The relationship between V_b and $< E_c >$ reveals a previously unexpected direct connection between the most important parameter of high field breakdown and the most basic physical properties of the crystal for wide bandgap semiconductors. Thus $< E_c >$ can be used as a guide in the choice of materials for use in electronic devices with optimised breakdown characteristics. This can be seen from equation (9) which can be stated generally as:

$$V_b = n < E_c > - m \qquad (11)$$

where m and n are constants.

We are therefore able to somewhat independently adjust within the same material the breakdown voltage and some other property of the bands (typically the bandgap) affecting, for example, the low-field transport properties, optical absorption, etc.. Figure 10 illustrates materials with (a) narrow bandgap and low $< E_c >$, (b) narrow bandgap and high $< E_c >$ and (c) wide bandgap and high $< E_c >$. Control of the breakdown properties is achieved by selection of appropriate semiconductor compounds, design of semiconductor alloys or strained layers, or "band-structure" engineering.

II. Device Structures - Design Concepts

We have shown hereinbefore that the concept of "band-gap engineering" of impact ionisation coefficients, by means of changing the bandstructure or potential discontinuity at the Brillouin-zone centre, fails for common materials such as GaAs. This is because both initial- and final-state carriers are scattered throughout the zone. In order to modify the ionisation coefficients, we must engineer the entire Brillouin zone. We replace the concept of "bandgap engineering" with "bandstructure engineering". Here we show applications of this concept to graded-gap, superlattice, multiple quantum well and other structures.

(a) Selection of Materials

The values of E_g and $< E_c >$ as shown in Table II can be used as criteria for selecting materials for fabricating semiconductor devices. For example, for high-speed, high-power transistors, the FET channel or bipolar base-collector junction should be fabricated from a material with high transient velocity (i.e. low effective mass and high intervalley separation, implying low E_g) and high breakdown voltage (implying high $< E_c >$). However E_g should be sufficiently large that Zener breakdown does not occur at lower field than avalanche breakdown (typically $E_g > \approx 0.8$eV). This also constrains the choice of material to the wide-bandgap semiconductors, as defined hitherto, which obey the scaling relation described by equation (9).

Figure 11 shows the values of E_g and $< E_c >$ plotted against the value of the lattice constant. Figure 11a is a plot for III-V compounds and Figure 11b is for Group IV elements and II -VI compounds. The additional data for HgTe in Figure 11b is from A. B. Chen and A. Sher, J. Vac. Sci. Technol. 21, 138 (1982). The energy gaps depend both on the volume of the crystal unit cell and on the chemical composition, decreasing with metallicity and increasing with ionicity. These trends are apparent in both E_g and $< E_c >$. The vertical lines connect E_g and $< E_c >$ for each material.

Wide-gap materials including Nitrides, ZnS, ZnSe, etc. also have large values of $< E_c >$ and hence large breakdown voltages, and hence are suitable for high temperature, high power electronics. The largest value of $< E_c > - E_g$ relative to E_g is exhibited by In-cation and N-anion compounds; hence InN (not shown) may be an attractive material for this purpose.

Thus, the data is Table II and Figure 11 gives the device designer basic information to enable a specific device to be constructed in accordance with the invention, with $< E_c >$ and E_g being selected according to the desired operating parameters for the device.

(b) Design of semiconductor alloys

Also, instead of using individual materials, alloys can be used. For example, a compound with small E_g ($\approx$ 0.8eV) and large $< E_c >$ (> 2eV) does not exist. However such a material can be created by designing appropriate lattice-matched or strained alloys. As an example, GaAs and InAs have bandgaps differing by more than 1eV, but quite similar values of $< E_c >$. Hence the alloy $In_{0.53}Ga_{0.47}As$ lattice matched to InP has a bandgap ($\approx$0.8eV) lower than that of GaAs (and hence has higher transient velocity), but has rather similar ionisation coefficients.

Another attractive material system is $Hg_xcd_{1-x}Te$, which can be grown with bandgaps between 0 eV and $\approx$ 1.8 eV. For a composition $x \approx 0.6$, the bandgap E_g is $\approx$ 0.8eV and $< E_c >$ is estimated as $\approx$ 2.5eV.

TableVI shows data for several III-V ternary alloys, lattice-matched to the substrate materials GaAs, InP, InAs and GaSb. The values of $< E_c >$ are determined by linear interpolation between binary constituents. The estimated breakdown voltage for a 1μm p-i-n diode is calculated from equation (9) (discussed in more detail hereinafter). Values in parenthesis are for narrow-bandgap materials for which equation (9) is not expected to be valid. A wide range of V_b can be obtained on each substrate material. The highest values of V_b are obtained in materials containing AlP or AlSb.

(c) Use of strained layers

Furthermore, the growth of strained pseudomorphic $In_xGa_{1-x}As$ on GaAs substrates results in compressive strain which increases the bandgaps. E_g is still smaller than in GaAs, resulting in confinement in the InGaAs (e.g. in GaAs/InGaAs pseudomorphic HEMTs); however $< E_c >$ is larger resulting in increased breakdown voltage compared to GaAs. This was observed in GaAs/InGaAs superlattices [J. P. R. David, M. J. Morley, A. R. Wolstenholme, R. Grey, M. A. Pate, G. Hill, G. J. Rees and P. N. Robson, Appl. Phys. Lett. 61, 2042 (1992)], although it was attributed to a different physical mechanism.

The above approach involves taking a narrow bandgap material and compressing it, causing an increase in E_g but also an increase in $< E_c >$ due to the positive value of the Brillouin-zone-averaged pressure coefficient. An opposite approach is to take a wide-bandgap, high- $< E_c >$ material and apply tensile strain. The rate of decrease with pressure of the bandgap is about 4 times that of $< E_c >$. Examples include $In_{0.5}Ga_{0.5}P$ on InP, or GaN on GaAs. The large lattice mismatch constrains the strained layer thickness to very small values, to avoid generation of dislocations.

(d) Graded-gap structures:

As previously discussed, graded gap materials have been used in devices such as APDs with minority carriers e. g. electrons generated in a wide band-gap absorption region being injected into the graded material, with an enhanced ionisation probability (relative to the hole probability at the same applied bias) due to carrier acceleration by the graded layer. In a typical case, carrier generation occurs in a narrow-gap layer, and carrier multiplication in a wide-gap graded layer. Hence a large potential barrier to the injection of carriers exists at the heterojunction, as in the case of the SAM APD. This can cause low efficiency and slow response due to carrier pile-up, as previously discussed.

In accordance with the present invention structures may be fabricated in which E_g and $< E_c >$ are independently controlled by compositional grading.

Examples of how E_g and $< E_c >$ can be independently controlled across the depth 2 of a semiconductor device is shown schematically in Figure 12. Figure 12a shows the band-edge profile where E_g is constant and $< E_c >$ is graded. Figure 12b shows the band-edge profile where $< E_c >$ is constant and

E_g is graded. Figure 12c shows the band-edge profile where both E_g and $< E_c >$ are graded.

(e) "Pseudo-alloy" superlattic s:

Superlattices in which the layer widths are sufficiently small compared to electron penetration lengths in the barriers (typically a few monolayers, or ≈ 1nm) behave in some respects as pseudoalloys, as far as optical absorption and low-field transport are concerned. An example of a superlattice pseudo-alloy is shown in Figure 13(a) and consists of multiple layers L1, L2 etc typically formed by molecular beam epitaxy, of materials with relatively wide and narrow bandgap, E_{g1}, E_{g2}. The pseudoalloy exhibits an effective bandgap E_g which is a function of E_{g1} and E_{g2}, and also a conduction band average energy $< E_c >$ as shown in Figure 13(a). For high-field transport, it has been shown [J. P. R. David, J. Allam, A. R. Adams, J. S. Roberts, R. Grey, G. Rees and P. N. Robson, Appl. Phys. Lett. **66**, 2876 (1995)] that pseudo-alloy behaviour occurs instead when the layer thicknesses do not exceed the carrier mean-free path at high energies (typically ≈ 10 nm). Hence for intermediate dimensions (1-10nm) the narrow-gap regions act as quantum wells for the absorption of light, whereas the breakdown characteristics are determined by $< E_c >$ which in turn is determined by the composition of the pseudoalloy. This is shown in Figure 13(b). Because the absorption edge is determined primarily by the bandgap of the well (plus the confinement energy), and the breakdown characteristics by the pseudoalloy composition, a greater difference between E_g and $< E_c >$ can be expected compared to a 'true' alloy. This concept is useful in cases where it is not desired to enhance the ionisation rates by means of the heterojunction discontinuities, and where sensitivity to long-wavelength light and high breakdown voltage are required. One example is for an optically-triggered IMPATT oscillator, for self-mixing optical heterodyne detection. Material systems for the fabrication of this structure include $In_{0.53}Ga_{0.47}As/InP$, etc. Thus, for a photodetector, a selection of the materials for the layers L1, L2, in a structure shown in Figure 13(b) allows E_g to be selected depending on the wavelength of the incoming light, and $< E_c >$ selected depending on the desired ionisation breakdown characteristics. Referring now to Figure 13(c), if the thickness of the layers L1, L2 exceed that which allows change carriers to relax their energy and momentum (≈ 50nm), then the carriers follow the variation in $< E_c >$ and the structure behaves as a series of hetero-junctions.

(f) Multiple quantum well:

So far, the scaling relation (9) discussed in the Analysis section hereinbefore, makes no statement regarding the relative size of the electron (α) and hole (β) ionisation coefficients, since the effective threshold for electrons and holes are not distinguished. The small differences in α and β which occur for most of the III-V materials are regarded as due to small differences in the electron and hole cross-sections for impact ionisation or phonon scattering. Nevertheless, it is possible to design quantum well structures in which either α or β is selectively enhanced. In the structures previously considered, the conduction-and valence-band discontinuities at the zone centre (ΔE_c and ΔE_v) were the parameters determining the behaviour, giving effective ionisation thresholds in the wells of $E_{th}^{(e)}$-ΔE_c and $E_{th}^{(h)}$-ΔE_v, for electrons and holes respectively.

In structures in accordance with the invention, it is the discontinuity in $< E_c >$, together with ΔE_v, which determines the ionisation probability. This will be explained with reference to Figure 14. In Figure 14, layers L1, L2 with relatively wide and narrow bandgaps between their conductive and valance bands are deposited to produce a series of quantum wells. Each well exhibits a discontinuity in the conduction and valance bands ΔE_v; ΔE_c. In accordance with the invention, the effective ionisation threshold in the wells becomes $< E_c > - \Delta < E_c > + \Delta E_v$ for electrons and $< E_c > - \Delta E_v$ for holes, where $< E_c >$ is the average conduction band energy in the well material, $\Delta < E_c >$ is the difference between $< E_c >$ for the well and barrier materials, and ΔE_v is the valence-band discontinuity at the zone centre. The heterojunction discontinuities can be estimated from the calculated energy bands using the dielectric mid-gap energy concept [M. Cardona and N.E. Christensen, Phys. Rev. B. 35, 6182 (1987)]. Two material systems have been identified as offering the largest selective enhancement of electrons over holes: $CdTe/Hg_xCd_{1-x}Te$ and $AlAs_{0.08}Sb_{0.92}/GaSb$. However, it has to be noted that these material systems are also the ones identified by Capasso [F. Capasso, in *Semiconductors and Semimetals* (ed. W.T. Tsang, Academic, New York) **22D** (1986) 1], based on an optimisation of the parameters $E_{th}^{(e)}$-ΔE_c and $E_{th}^{(h)}$-ΔE_v. Thus, in accordance with the invention, a quasi-independent control of $\Delta < E_c >$ and ΔE_c allows optimisation of the structure both for optical absorption and carrier transport, and for ionisation rate enhancement.

Examples of devices which make use of these design considerations will now be described.

(III) Detailed Examples of Device Structures

FETs

Referring to Figure 15, a first embodiment of a HEMT, according to the present invention, comprises a substrate 1, a channel layer 2 on the substrate 1, a supply layer 3 on the channel layer 2, n+ source and drain contact regions

4, 5 and a gate 6 formed on the supply layer 3, and source and drain electrodes 7, 8 forming ohmic contacts to the source and drain contact regions 4, 5 respectively. In use, a non-uniform field is produced in the channel 2, which is relatively low underneath most of the gate 6, but relatively high at the drain end of the gate. In accordance with the invention, the composition of the channel 2 can be tailored to optimise the characteristics of both the high field and low field regions of the channel.

The channel layer 2 has a low electric field region 2a and a high electric field region 2b that are made of materials with different values of $< E_c >$. In the high field region 2b, the value of $< E_c >$ is selected e.g. from the values shown in Table II, to be relatively high to avoid the risk of avalanche breakdown under the effect of the field produced beneath the gate 6. The material for the low field region 2a is selected to have a low value of E_g, in order to maximise the effective carrier velocity under the gate.

In one implementation, the low electric field region 2a of the channel layer 2 comprises $In_{0.53}Ga_{0.47}As$ and the high electric field region 2b comprises $In_{0.52}Al_{0.48}As$. The risk of impact ionisation in the high electric field region 2b is therefore greatly reduced by the relatively high $< E_c >$ value. However, the relatively low value of E_g in the low electric field region 2a maximizes the effective carrier velocity under the gate as well as providing a low source access resistance. Also, the potential barrier between the electron supply layer 3 and the channel 2 is large, leading to high sheet carrier density and high modulation efficiency.

Referring to Figure 16, a second embodiment of a HEMT, according to the present invention, comprises a substrate 1, a channel layer 2 on the substrate 1, an n-type supply layer 3 on the channel layer 2, n+ source and drain contact regions 4, 5 and a gate 6 formed on the supply layer 3, and source and drain electrodes 7, 8 forming ohmic contacts to the source and drain contact regions 4, 5 respectively.

The composition of the channel layer 2 is graded from $In_{0.53}Ga_{0.47}As$ under the source electrode 7 to $In_{0.52}Al_{0.48}As$ under the drain electrode 8. The grading of the composition of the channel layer 2 is arranged such that the value of $< E_c >$ increases from the source electrode end to the drain electrode end. By grading the channel layer composition, rather than using discrete regions, the balance between carrier mobility and breakdown field strength can be optimised throughout the length of the channel layer 2, and any barrier that may occur at the junction between regions 2a, 2b in Figure 15 is avoided.

In a modification, the supply layer 3 is also graded, to optimise the combination of high carrier concentration in the low field region and control of the real space transfer in the high field region. The graded layer may be lattice matched to the substrate (e.g. $In_{0.53}Ga_{0.47}As$ graded to $In_{0.52}Al_{0.48}As$ on InP substrate), or may be pseudomorphically strained with a constant strain parameter, or may be strained with a strain which varies along the channel due to the change in composition. Alternatively, the strain in the channel can be generated and controlled by means of a surface stressor layer, which has a different lattice constant to the substrate. The strain can be varied by appropriate control of the lattice constant of the stressor layer. The strain in the channel, however it is achieved, modifies the bandstructure and hence can be used to tailor materials for operation at low or high fields.

Non-alloyed source and drain contacts can be used, if the supply layer 3 is also suitably graded in terms of $< E_c >$. The grading of the supply layer 3 needs to be such that the heterojunction discontinuity between the supply and channel layers 2,3 is reduced beneath the source and drain electrodes 7,8. Reducing this discontinuity results in reduced contact resistance.

Referring to Figure 17, a third embodiment of a HEMT, according to the present invention, comprises an InP substrate 1, a channel layer 2 on the substrate 1, an n-type supply layer 3 on the channel layer 2, a source contact region 10 extending up from the channel layer 2, a gate 6 formed on the supply layer 3, source electrode 7, forming an ohmic contact to the source contact region 10, and a drain electrode 11, forming an unannealed Schottky contact to the supply layer 3.

The channel layer 2 is formed from InAs, which has a small bandgap, under the source contact. The source contact region 10 is also formed from InAs and, consequently, the device of Figure 17 has both a low source access resistance and a low source contact resistance. The channel layer 2 is graded in terms of $< E_c >$ in a manner similar to that of the embodiment of Figure 14.

Carriers in the high-field gate-drain region are not confined to the two-dimensional electron gas (2DEG). Therefore, a "spiking" ohmic contact is not required at the drain electrode 11, in order to extract carriers from the potential well. Instead, the present embodiment uses an unannealed Schottky contact, trading increased potential drop across the channel for reduced contact resistance.

Referring to Figure 18, a fourth embodiment of a HEMT, according to the present invention, comprises an InP substrate 1, a channel layer 2 on the substrate 1, an n-type supply layer 3 on the channel layer 2, n+ source and drain contact regions 4, 5 and a gate 6 formed on the supply layer 3, and source and drain electrodes 7, 8 forming ohmic contacts to the source and drain contact regions 4, 5 respectively.

The composition of the channel layer 2 is graded along its length to induce a varying strain in its lattice. This strain affects the value of $< E_c >$. Accordingly, the grading of the composition of the channel layer 2 can arranged such that $< E_c >$ increases from the source electrode end to the drain electrode end, in order to optimise the voltage breakdown/

carrier mobility relationship along the channel.

The required strain in the channel layer can also be externally applied.

Referring to Figure 19, the manufacture of a fifth embodiment of the present invention will now be described. A HEMT is produced by growing a first relatively thick layer 12 $In_{0.53}Ga_{0.47}As$ on an InP substrate 1. Thereafter, a plurality of layers 13, each a few atoms thick, are epitaxially grown over the first layer 12. The composition of the layers 13 varies and is carefully selected such that the value of $< E_c >$ for each new layer is greater than that of the previously grown layer according to a predetermined design. Alternatively, a graded layer can be used. Finally, a second relatively thick layer 14 of $In_{0.52}Al_{0.48}As$ is epitaxially grown over the uppermost of the layers 13.

The multilayer or graded structure thus produced, is cleaved vertically into slivers, one of which is shown in Figure 19. The ends of the layers 12, 13, 14 are exposed on the cleaved faces of the sliver and form a graded channel layer 2. An n-type supply layer 3 is then epitaxially grown on one of the cleaved faces of the sliver. Then, source and drain contact regions 4, 5 and a gate 6 are formed on the supply layer 3. Finally, source and drain electrodes 7, 8 are formed on the contact regions 4, 5.

A plurality of HEMTs may be formed side-by-side on one sliver which can then be cleaved to provide separate devices. The remnant of the substrate 1 may also be removed. After separation, the devices can be encapsulated in the normal way.

Another example of FET manufactured in accordance with the method of the invention is shown in Figure 20. In this example, devices are formed in a V-groove in the substrate. Initially, a vertically graded layer 15 is grown on substrate 1, which is overlaid by a further layer 16 of the same conductivity type as the substrate. A V-groove 17 is formed in the device. First and second transistors are formed on opposite sides of the V-groove. A source region 18 is formed in the bottom of the groove and gate regions 19a, 19b are formed on the sides of the groove. Drains 20a, 20b for the respective transistors are formed in contact with regions 16a, 16b. The grading of the channel regions 16 is controlled to optimise breakdown voltage and bandgap in the manner previously described.

The FETs according to the invention have been described with reference to n-channel devices. However, it will be appreciated that it can equally be applied to p-channel devices.

Bipolar Transistors

Figure 21 shows a general n-p-n polar transistor structure that consists of a substrate 21 overlaid by n^+ contact layer 22, an n-type collector layer 23, a p-type base 24, an n-type emitter layer 25 and a n^+ contact layer 26. Base, collector and emitter metallisation 27, 28 and 29 is provided on the base 24 and the contact layers 22, 26. This HBT structure, whilst shows as an n-p-n transistor could equally be a p-n-p device as will be readily apparent to those skilled in the art. The device may be a single heterojunction HBT e.g. with a heterojunction between the n-type emitter layer 25 and the base 24, or a double heterojunction HBT, with a heterojunction also between the base 24 and the collector 23.

The energy band diagrams for conventional single and double heterojunction HBTs are shown in Figure 22(a) and (b) respectively.

In accordance with the invention, the materials for the emitter, base and collector may be chosen according to the principles discussed hereinbefore, so that the breakdown characteristics of the device can be selected independently of the characteristics of the conduction band. In Figure 22(c) the energy bands for a single heterojunction HBT in accordance with the invention is shown. Figure 22(d) shows a corresponding energy band diagram for a HBT according to the invention with a graded collector.

Figure 23(a)-(d) illustrate material systems that correspond to the energy band diagrams shown in Figures 22(a)-(d) respectively.

Figure 23 shows GaAs-based structures, with Al_xGa_{1-x} or $(Al_xGa_{1-x})_{0.52}In_{0.48}P$ collector and GaAs base. Conventionally, the collector may be (a) GaAs or for the double heterojunction (b) $Al_xGa_{1-x}As$ or $Ga_{0.52}In_{0.48}P$. Figure 24 shows corresponding InP-based devices; the emitter is InP or $Al_{0.48}In_{0.52}As$, the base is $In_{0.53}Ga_{0.47}As$ and the collector is (a) $In_{0.53}Ga_{0.47}As$, or the double heterojunction structure is InP or (b) $Al_{0.48}In_{0.52}As$. Note that, in Figure 24(b), the electron injection efficiency from the base to the collector is reduced by the large conduction-band discontinuity; as mentioned above.

The breakdown voltage may be increased by choosing a collector material with high $< E_c >$. For GaAs based structures, this may be $Al_{0.52}In_{0.48}P$, or $AlP_{0.70}Sb_{0.30}$. Furthermore, to avoid the problem of reduced injection efficiency, the base and collector materials may be chosen so that the conduction band discontinuity between them is zero. This occurs, for example, for the material combination $Al_{0.12}Ga_{0.88}As/Ga_{0.52}In_{0.48}P$ [Kim et al., Appl. Phys. Lett. 68, 3488 (1996)] - see structure in Figure 23(c). For InP based structures, $AlP_{0.39}Sb_{0.61}$ offers a high $< E_c >$ (Figure 24(c)).

Structures in which the collector material is compositionally graded from the base material to a material with high $< E_c >$ offer both high injection efficiency and low electron initiated ionisation probability. Figure 23(d) shows a GaAs/$Ga_{0.52}In_{0.48}P$ graded layer, and Figure m(d) shows an $In_{0.53}Ga_{0.47}As/InP$ or $In_{0.53}Ga_{0.47}As/Al_{0.48}In_{0.52}As$ structure. In all the GaAs base structures mentioned above, improved base resistance, base transit time and base hole confinement

can be achieved using a strained pseudomorphic $In_xGa_{1-x}As$ base.

APDs

Referring to Figure 25, an APD is shown in cross section and consists of an n^+ substrate 30 on which is formed an i-layer 31, which itself is overlaid by a p-type region consisting a p-type absorption layer 32 that absorbs incoming light, and a p^+ contact region 33. Metallic contacts 34, 35 are formed on the p^+ region 33 and the n^+ region 30. The overall layer structure of the device is conventional and reference is directed to Capasso *(ibid)*. The band structure for a conventional APD is shown in Figure 26. The various semiconductor layers exhibit a valance band E_v and a conduction band E_c, with a band gap E_g between them. In order to achieve satisfactory low dark current in the layer 31, the bandgap E_g of the layer needs to be relatively high. However, this renders the layer relatively insensitive to incoming light of long wavelength and so no significant photocurrent is produced in the layer 31. The wavelength dependence of the photocurrent generation is a function of the bandgap E_g which needs to be made smaller in order to achieve satisfactory production of photogenerated charge carriers in a useful wavelength range, such as near-infrared. This leads to a problem in that there is a band discontinuity at the heterojunction between the p-type absorption layer 32 and the undoped multiplication layer 31. The band edge produces a barrier 35 which prevents charge carriers passing between the layers and so electrons produced in the p-type absorption layer 32 tend to pile up at the junction 35 before entering the multiplication layer 31.

Also, as previously explained, the undoped multiplication layer 31 tends to produce a relatively high multiplication noise due to the fact that the material exhibits substantially similar ionisation coefficients α, β for electrons and holes.

Graded-Gap APDs

Figure 27 is a band diagram of the device when the multiplication layer 31 is graded in the manner described in US Patent 4 383 269 discussed previously. The band edges E_c and E_v have unequal slopes in the multiplication region 31, resulting in preferential amplification of electrons, thereby reducing noise and producing a more stable gain. However, the wide gap absoprtion layer is no longer sensitive to a useful wavelength range, because the wavelength sensitivity is a function of the band gap Eg.

This can be overcome by the prior art arrangement shown in Figure 28, by making the band gap of the absorption layer 32 narrower than that shown in Figure 27, but with the disadvantage that the barrier 35 at the junction between the layers 31, 32 produces a build up of charge at the junction.

These problems are overcome in accordance with the invention by providing a band structure in the APD as shown in Figure 29. In accordance with the invention, the average conduction band energy $< E_c >$ is configured to control the ionisation characteristics of the device and the band gap for the light absorption layer 32 is configured separately. The materials used in the p-type absorption layer 32 and the undoped multiplication layer 31 are selected so that their values of E_g produce minimal discontinuities in the conduction and valance bands E_v and E_c at the heterojunction between the layers. In this way, the barrier 35 shown in Figures 26 and 27 is avoided. Furthermore, the bandgap E_g for the p-type absorption layer 32 is chosen so that it is sufficiently small to be sensitive to a useful wavelength range for incoming light e.g. near-infrared.

Additionally, in accordance with the invention, the materials are chosen so that the value of the average energy $< E_c >$ has a characteristics shown by dotted line 36 in Figure 29. The material chosen for the p-type absorption layer 32 is selected to have a relatively high value 36 of average conduction band energy $< E_c >$, relative to the valance band energy E_v. As a consequence, the risk of ionisation breakdown in the absorption layer is minimised. However, in the undoped multiplication layer 31, the material is configured so that the value 36 of $< E_c >$ is graded progressively through the thickness of the layer. As previously explained, the grading results in an increase ionisation α for electrons as compared with the corresponding coefficient β for holes, which reduces noise and improves amplification stability. Furthermore, the material chosen for the layer 31 is selected so that its band gap E_g substantially matches the band gap E_g of the layer 32, so that no potential barrier (such as barrier 35 - Figure 26) is produced at the heterojunction between the layers 31, 32. Thus, photo-produced charge carriers from the layer 32 can readily flow into the layer 31, for avalanche multiplication without a charge carrier build up at the heterojunction between the layers.

By making reference to the materials listed in Table II hereinbefore, those skilled in the art will readily be able to determine suitable materials for use in the APD.

Pseudoalloy Superlattice

Figure 30 illustrates a cross-section of a quantum well APD that comprises a GaAs substrate 37 with an overlying n^+ contact layer 38 itself overlaid by an undoped superlattice absorption and multiplication layer 39. The pseudoalloy superlattice consists of a structure that comprises overlying layers of GaAs and $In_xGa_{1-x}As$ several monolayers thick,

deposited by conventional techniques such as molecular beam epitaxy. As is known in the art, the resulting structure comprises a plurality of quantum wells. The well structure 39 is overlaid by a p^+ contact layer of GaAs material 40. Metallic, ohmic contacts 41, 42 are provided on the layer 40 and the n^+ contacts layer 38.

The band structure of the device is shown in Figure 31. The modulation doped structure 39 forms a series of quantum wells W_{1e}, W_{2e}, W_{1h}, W_{2h} etc. In response to incident light, electron hole pairs are produced and the electrons and holes initially reside in the quantum wells. The voltage applied to the contacts 41, 42 results in the field across the layer 39 and as a result, the electrons and holes shift out of the wells and photo multiplication occurs as a result of ionisation in the material of the superlattice.

In accordance with the invention, the degree of ionisation is determined by the level of $< E_c >$, which is shown as a dotted line 43 in Figure 31. By an appropriate selection of the materials used to form the superlattice, the value of $< E_c >$ can be suitably selected. This can be achieved quasi-independently of the parameters of the quantum wells. It will be understood that the dimensions of the quantum wells determine the wavelength sensitivity of the structure and so in accordance with the invention, the wells can be engineered to achieve a particular wavelength sensitivity and the value of $< E_c >$ can be suitably selected to provide desired ionisation characteristics. This contrasts with the prior art in which the relative values of E_c and E_v were controlled in order to determine both the band gap of the well and the ionisation characteristics.

The device shown in Figure 30 can be used for detecting light at a wavelength of 1.3μm. GaAs has the lowest bandgap of any lattice-matched bulk or alloy semiconductor of the same lattice constant, but is limited to detecting wavelengths of less than ≈0.85μm. However this bandgap can be lowered by the provision of the pseudomorphic $In_xGa_{1-x}As$ layers in the region 39, increasing the detectable wavelength to 1.3μm. Hence an $In_xGa_{1-x}As$ / GaAs strained superlattice structure as shown in Figure 30 can be selected to exhibit an increased breakdown voltage as a function of $< E_c >$, as well as an increased maximum detectable wavelength.

Referring now to Figure 32, another embodiment of SAM-APD is shown, which is similar to the device for Figure 30. The device of Figure 32 additionally includes an undoped multiplication layer 44 under the absorption layer 39, so that the light absorption function is performed by strained layer superlattice 39 and avalanche charge carrier multiplication occurs in the layer 44. For GaAs, the ionisation coefficient α for electrons is greater than the corresponding coefficient β for holes so electrons are injected into the multiplication layer 44, and are multiplied by the avalanche effect.

The band structure of the device of Figure 32 is shown in Figure 33. In the region of the strained superlattice 39, the value of $< E_c >$ is relatively high, whereas in the region of the multiplication layer 44, the average energy is of a lower value, so as to promote ionisation. In one example, the layer 44 comprises GaAs material and the superlattice region 39 comprises alternate layers of GaAs and $In_xGa_{1-x}As$ material where $x < 0.3$.

Referring to Figure 34, there is a risk that a dark current will occur as a result of Zener tunnelling between quantum wells in the superlattice structure 39. This can be suppressed as shown in Figure 24(b) by forming the superlattice 39 of alternate layers of $Al_xGa_{1-x}As$ and $In_xGa_{1-x}As$ material. Carrier trapping in the quantum wells may be avoided by using "chirped" superlattices in which either electrons or holes or both tunnel resonantly out of the wells by way of quantised energy levels in adjacent, narrow wells. This is shown in Figure 34(c). It will be understood that the periodicity of the superlattice will be modulated spatially in order to achieve the desired chirped quantum well configuration.

Multiple Quantum Well APD

A multiple quantum well or superlattice avalanche photodiode is described in *Chin, Holonyak & Stillman, Electronics Letters, vol. 16, p. 648 (1980).* An improved device of this type may be formed by forming alternating layers of $In_{0.48}Ga_{0.52}P$ and $Al_xGa_{1-x}As$ where x is approximately 0.35. Such a device will have substantially constant E_g throughout the alternating layers but $< E_c >$ will be modulated. The advantages of such a device is that secondary or photogenerated electrons are not trapped in the wells.

The impact ionisation of a multilayer heterojunction system, forming a superlattice or multiple quantum well, may be enhanced by means of energy gained at a heterojunction by electrons crossing from a region of high $< E_c >$ to a region of low $< E_c >$. Such a structure can be formed by alternating layers of GaAs and $(Al_xGa_{1-x})_{0.52}In_{0.48}P$. In this structure there is a significant discontinuity in $< E_c >$ between the two materials.

IMPATTs

Conventionally, in certain IMPATT structures such as Read diodes, Hi-lo diodes, and Lo-hi-lo diodes, the avalanche multiplication and drift occur in regions of different doping, such that a high field exists in the avalanche region and a relatively low field in the drift region. These structures are most amenable to optimisation by using a method in accordance with the invention. By suitable choice of materials for the two different layers, the output power is increased by maximising the avalanche breakdown voltage, while the operating frequency is increased by maximising the electron velocity. The former is according to the invention by selecting a material with a large value of $< E_c >$, and the latter is

achieved by selecting a material which also exhibits low effective mass and high saturated drift velocity.

Figure 35 shows IMPATT devices corresponding to Read (a), Hi-lo (b) and Lo-hi-lo (c) structures. Figure 36 shows only the avalanche and drift region, omitting any surrounding or intermediate layers. Referring to Figures 35, 36 each structure consists of a substrate 45 with an n^+ ohmic contact 46 overlaid by an undoped drift region 47 on a n-type avalanche region 48. A p-type contact region 49 contacts the region 48. Metallic contacts 50, 51 are provided on the layers 46, 50.

In structure (a), the multiplication layer is formed from an $In_xGa_{1-x}As/GaAs$ pseudoalloy strained layer superlattice, as described above, in order to increase the value of $< E_c >$ and hence V_b. In structure (b), the multiplication layer is $Ga_{0.52}In_{0.48}P$ or $Al_{0.52}In_{0.48}P$, which materials have been experimentally demonstrated to exhibit a high breakdown voltage. In structure (c) and (d), which is formed on an InP substrate 45, the drift region is $In_{0.53}Ga_{0.47}As$ which exhibits a high saturated carrier velocity. The multiplication layer is InP in case (c) or $AlP_{0.39}Sb_{0.61}$ in structure (d), for even higher breakdown voltage. These structures exhibit increased power-bandwidth product compared to known structures.

Other Specific Devices

p-i-n Microwave Switch

Referring to Figure 37, a p-i-n diode comprises a p-type region 52, an intrinsic region 53 and an n-type region 54. Such diodes are used in microwave switching circuits. The switching speed is given approximately by $W/2v_s$, where v_s is the saturation velocity across the intrinsic region 53 and W is the width of the intrinsic region 53. Thus, it can be seen that it is desirable for W to be as small as possible for fast switching. However, reducing W reduces also the reverse breakdown voltage of the diode. According to the present invention, the reverse breakdown voltage can be increased for a given value of W, thereby allowing an increase in switching speed without the penalty of reduced breakdown voltage.

For a p-i-n diode having an intrinsic region width W of 1μm it has been found that the following relationship exists:

$$V_b = 45.8\langle E_c \rangle - 46.3 \text{ volts} \qquad (12)$$

Thus, the reverse breakdown voltage for the diode can be varied between 49.6V in the case where the diode is formed of AlSb ($< E_c >$ - 2.09eV), to 64.4V in the case where the diode is formed of AlAs ($< E_c >$ - 2.41eV), to 102.4V in the case where the diode is formed of AlP ($< E_c >$ - 3.24eV), merely by selecting the material on the basis of $< E_c >$.

According to the prior art, where V_b is determined on the basis of equation (3) the width of the intrinsic region W would be over-estimated resulting in a slower switching speed than was necessary. For instance, an AlP p-i-n diode with W- 1μm would have been expected to have a breakdown voltage of 68V on the basis of a bandgap of 2.50eV (Sze S.M. *Physics of Semiconductor Devices 2nd Edition* (Wiley, 1981)).

Voltage Reference

A simple example of a device, in which a predetermined breakdown voltage needs to be achieved, is an avalanche diode for use as a voltage reference. In the manufacture of such devices it is desirable to be able to control the fabrication process such that a diode having the desired characteristics is produced. According to the present invention, either doping concentration can be controlled on the basis of the $< E_c >$ for the material used to produce a device having a predetermined breakdown voltage or the material use can be selected on the basis of its $< E_c >$ to give a predetermined breakdown voltage for a given doping concentration.

It is emphasised that the present invention is applicable to the production of any type of device where the avalanche breakdown properties are important. In some devices, such as rectifying diodes, the highest possible breakdown voltage is desirable. In others, such as APDs diodes, a high impact ionisation coefficient is desirable. In still other devices, such a voltage reference diodes, a specific breakdown voltage is required. Thus, it can be seen that the present invention provides for improved devices of many disparate types, including diodes and all forms of transistor.

Table I

Material	E_Γ (eV)	E_L (eV)	E_X (eV)	$\langle E_C \rangle$ (eV)	V_b (V)
GaAs	1.43	1.71	1.90	1.75	33.6
$Ga_{.85}Al_{.15}As$	1.62	1.80	1.92	1.83	38.9
$Ga_{.7}Al_{.3}As$	1.81	1.90	1.95	1.91	44.5

Table I (continued)

Material	E_Γ (eV)	E_L (eV)	E_X (eV)	$\langle E_C \rangle$ (eV)	V_b (V)
$Ga_{.6}Al_{.4}As$	1.95	1.96	1.97	1.96	49.0
$Ga_{.5}Al_{.5}As$	2.10	2.03	2.00	2.03	52.4
$Ga_{.4}Al_{.6}As$	2.25	2.09	2.03	2.09	56.2
$Ga_{.52}In_{.48}P$	1.90	2.10	2.20	2.11	61.7
$(Al_{.24}Ga_{.76})_{.52}In_{.48}P$	2.05	2.18	2.22	2.17	65.3
$(Al_{.50}Ga_{.50})_{.52}In_{.48}P$	2.21	2.27	2.25	2.25	69.2
$(Al_{.70}Ga_{.30})_{.52}In_{.48}P$	2.33	2.34	2.26	2.30	72.3
$Al_{.52}In_{.48}P$	2.51	2.44	2.29	2.38	76.0

Table II

material	a_0	E_Γ			E_L			E_X			E_g	$<E_c>$
	(Å)	(eV)			(eV)			(eV)			(eV)	(eV)
		th[a]	cor[b]	exp[c]	th[a]	cor[b]	exp[c]	th[a]	cor[b]	exp[c]		
C	3.57	7.60	7.33	7.30							5.48	
Si	5.43	3.43	3.40	3.40	2.36	2.26		1.47	1.43	1.30	1.17	2.09
Ge	5.66	0.71	0.84	0.89	0.75	0.88	0.74	1.23	1.22	1.30	0.74	0.97
BN	3.62	11.40	10.91		12.40	10.84		6.30	5.81	6.20	5.81	8.96
BP	4.54	4.40	4.31	5.00	4.60	4.17		2.00	1.91		2.04	3.34
BAs	4.78	4.00	3.94		3.30	3.06		1.93	1.85		1.55	2.72
AlN	4.35	6.00	5.82		9.30	8.19		4.90	4.54		4.54	6.52
GaN	4.50	3.10	3.09	3.25	6.20	5.54		4.70	4.36		3.25	4.79
AlP	5.45	4.38	4.30	3.62	3.90	3.58		2.59	2.45	2.50	2.50	3.24
AlAs	5.65	2.88	2.88	3.13	2.91	2.73	2.36	2.14	2.04	2.23	2.23	2.41
AlSb	6.14	2.23	2.27	2.32	1.84	1.82	2.33	1.64	1.59	1.68	1.68	2.09
GaP	5.45	2.85	2.85	2.89	2.67	2.52	2.64	2.55	2.41	2.39	2.39	2.58
GaAs	5.65	1.22	1.32	1.52	1.64	1.64	1.74	2.01	1.92	1.90	1.52	1.77
GaSb	6.10	0.62	0.75	0.82	0.79	0.92	0.92	1.15	1.15	1.15	0.80	0.99
InP	5.87	1.44	1.53	1.42	2.28	2.19	2.03	2.58	2.44	2.38	1.42	2.09
InAs	6.04	0.31	0.46	0.41	1.43	1.47	1.55	2.01	1.92		0.41	1.51
InSb	6.47	0.08	0.24	0.23	0.76	0.89		1.50	1.46	1.79	0.23	1.03
$Al_{.5}Ga_{.5}As$	5.65	2.06	2.11	2.09	2.25	2.17	2.03	2.05	1.96	1.97	2.09	2.01
$In_{.53}Ga_{.47}As$	5.87	0.80	0.92	0.81	1.63	1.64		2.07	1.98		0.81	1.68
ZnS	5.41	3.98	3.92	3.80	5.28	4.75		5.14	4.76		3.80	4.65

[a]theoretical (ab-initio quasiparticle) energies of Louie and coworkers.

[b]theoretical energies corrected for systematic errors.

[c]experimental energies collated by Louie and coworkers.

Table II (continued)

material	a_0	E_Γ			E_L			E_X			E_g	$<E_c>$
	(Å)	(eV)			(eV)			(eV)			(eV)	(eV)
		th[a]	cor[b]	exp[c]	th[a]	cor[b]	exp[c]	th[a]	cor[b]	exp[c]		
ZnSe	5.67	2.84	2.84	2.96	4.14	3.78		4.41	4.10		2.96	3.78
ZnTe	6.09	2.57	2.59	2.71	3.07	2.87		3.47	3.24		2.71	2.97
CdS	5.82	2.83	2.83	2.55	4.82	4.36		5.08	4.70		2.55	4.30
CdSe	6.05	2.01	2.06	1.90	3.87	3.55		4.37	4.06		1.90	3.56
CdTe	6.48	1.76	1.83	1.92	2.84	2.67		3.46	3.24		1.92	2.78
HgTe[d]	6.46	-0.30	-0.11		1.28	1.34		2.35	2.23		0.00	1.49

[a]theoretical (ab-initio quasiparticle) energies of Louie and coworkers.

[b]theoretical energies corrected for systematic errors.

[c]experimental energies collated by Louie and coworkers.

[d]A. B. Chen and A. Sher, J. Vac. Sci. Technol. 21, 138 (1982)

Table III

material	a_0	E_0			E_1			E_2			$<E_G>$
	(Å)	(eV)			(eV)			(eV)			(eV)
		th[a]	cor[b]	exp[c]	th[a]	cor[b]	exp[c]	th[a]	cor[b]	exp[c]	
C	3.57	7.60	7.33	7.30	13.60	13.11	14.40	13.10	12.51	12.60	12.84
Si	5.43	3.43	3.40	3.40	3.64	3.67		4.49	4.46	4.40	3.93
Ge	5.66	0.71	0.84	0.89	2.18	2.28		4.45	4.42	4.63	2.90
BN	3.62	11.40	10.91		14.60	14.06		11.80	11.30		12.63
BP	4.54	4.40	4.31	5.00	6.50	6.38	8.00	6.50	6.34	6.90	6.11
BAs	4.78	4.00	3.94		5.30	5.24		6.43	6.27		5.46
AlN	4.35	6.00	5.82		9.90	9.60		7.00	6.81		8.08
GaN	4.50	3.10	3.09	3.25	7.30	7.14		7.70	7.46		6.75
AlP	5.45	4.38	4.30	3.62	4.75	4.72		4.90	4.84		4.71
AlAs	5.65	2.88	2.88	3.13	3.90	3.91	3.92	4.58	4.54	4.64	4.09
AlSb	6.14	2.23	2.27	2.32	2.90	2.96	2.89	4.18	4.17		3.33
GaP	5.45	2.85	2.85	2.89	3.83	3.85	3.91	5.33	5.24	5.39	4.34
GaAs	5.65	1.22	1.32	1.52	2.92	2.98	3.15	4.88	4.82	4.81	3.57
GaSb	6.10	0.62	0.75	0.82	1.93	2.05	2.02	3.88	3.89	4.01	2.62
InP	5.87	1.44	1.53	1.42	3.30	3.34	3.18	4.96	4.90	4.58	3.48
InAs	6.04	0.31	0.46	0.41	2.56	2.64	2.59	4.50	4.47		3.05
InSb	6.47	0.08	0.24	0.23	1.72	1.85		4.06	4.06	4.19	2.47
$Al_{.5}Ga_{.5}As$	5.65	2.06	2.11	2.09	3.41	3.45		4.73	4.68		
$In_{.53}Ga_{.47}As$	5.87	0.80	0.92	0.81	2.81	2.88		4.71	4.66		
ZnS	5.41	3.98	3.92	3.80	6.06	5.96	5.81	7.20	6.99	6.60	5.86

[a]theoretical (ab-initio quasiparticle) energies of Louie and coworkers.

[b]theoretical energies corrected for systematic errors.

[c]experimental energies collated by Louie and coworkers.

Table III (continued)

material	a_0	E_0			E_1			E_2			$<E_G>$
	(Å)	(eV)			(eV)			(eV)			(eV)
		th[a]	cor[b]	exp[c]	th[a]	cor[b]	exp[c]	th[a]	cor[b]	exp[c]	
ZnSe	5.67	2.84	2.84	2.96	4.95	4.91	5.02	6.49	6.33	6.42	5.29
ZnTe	6.09	2.57	2.59	2.71	3.95	3.96		5.63	5.52	5.41	4.38
CdS	5.82	2.83	2.83	2.55	5.50	5.43		6.82	6.64		5.56
CdSe	6.05	2.01	2.06	1.90	4.58	4.56		6.15	6.01		4.79
CdTe	6.48	1.76	1.83	1.92	3.57	3.60	3.72	5.24	5.16		3.96
HgTe[d]	6.46	-0.30	-0.11		1.96	2.07		4.68	4.64		2.76

[a]theoretical (ab-initio quasiparticle) energies of Louie and coworkers.

[b]theoretical energies corrected for systematic errors.

[c]experimental energies collated by Louie and coworkers.

[d]A. B. Chen and A. Sher, J. Vac. Sci. Technol. 21, 138 (1982).

Table IV

Material	Bandstructure				Breakdown
	E_g (eV)	E_Γ (eV)	$<E_c>$ (eV)	$<E_G>$ (eV)	V_b (V)
Si	1.17	3.40	1.85*	3.98*	34.3[a]
Ge	0.74	0.89	0.97	2.90	19.7[b]
GaP	2.39	2.85	2.58	4.34	61.4[c]
InP	1.42	1.42	2.09	3.48	46.5[d]
GaAs	1.52	1.52	1.77	3.57	33.6[e]
$Ga_{0.47}In_{0.53}As$	0.81	0.81	1.65	3.28	33.2[f]
$Al_{0.48}In_{0.52}As$	1.55	1.55	1.96	3.53	46.5[g]
$GaAs_{0.88}Sb_{0.12}$	1.44	1.44	1.68	3.46	26.5[h]
$Al_{0.06}Ga_{0.94}Sb$	0.87	0.87	1.06	2.66	22.0[i]
$Al_{0.28}Ga_{0.72}Sb$	1.06	1.06	1.30	2.81	25.2[j]
GaAs	1.52	1.52	1.77	3.57	33.6[k]
$Al_{0.15}Ga_{0.85}As$	1.72	1.72	1.87	3.65	38.9[k]
$Al_{0.3}Ga_{0.7}As$	1.93	1.93	1.96	3.73	44.5[k]
$Al_{0.4}Ga_{0.6}As$	2.06	2.06	2.03	3.78	49.0[k]
$Al_{0.5}Ga_{0.5}As$	2.07	2.20	2.09	3.83	52.4[k]
$Al_{0.6}Ga_{0.4}As$	2.10	2.34	2.15	3.88	56.2[k]
$Ga_{0.52}In_{0.48}P$	2.18	2.18	2.34	3.93	61.7[k]
$(Al_{0.24}Ga_{0.76})_{0.52}In_{0.48}P$	2.37	2.37	2.43	3.99	65.3[k]
$(Al_{0.50}Ga_{0.50})_{0.52}In_{0.48}P$	2.41	2.55	2.52	4.04	69.2[k]
$(Al_{0.75}Ga_{0.25})_{0.52}In_{0.48}P$	2.43	2.74	2.61	4.10	72.3[k]
$Al_{0.52}In_{0.48}P$	2.44	2.92	2.70	4.15	76.0[k]

*In the case of Si, the Γ valley is assumed not to play any role, hence $<E> \approx (1/7)(3E_X+4E_L)$.

[a] C.A.Lee, R.A.Logan, R.L. Batdorf, J.J.Kleimack and W.Wiegmann, Phys. Rev. 134, A761 (1964)
[b] S. L. Miller, Phys . Rev. 99, 1234 (1965)
[c] R. A. Logan and White, J. Appl. Phys. 36, 3945 (1965)
[d] C. A. Armiento, S. H. Groves, and C. E. Hurwitz, Appl. Phys. Lett. 35, 333 (1979)
[e] G. E. Bulman et al., IEEE Electron Dev. Lett. 4, 181 (1983)
[f] average value of: T. P. Pearsall, Appl. Phys. Lett. 36, 218 (1980); F. Osaka, T. Mikawa and T. Kaneda, IEEE J. Quantum Electronics 21, 1326 (1985); J. Urquhart, D. J. Robbins, R. I. Taylor and A. J. Mosely, Semiconductor Science and Technol. 7, 789 (1990); J. Bude and K. Hess, J. Appl. Phys. 72 (1992) 3554; C. Canali, C. Forzan, A. Neviani, L. Vendrame, E. Zanoni, R. A. Hamm, R. J. Malik, F. Capasso and S. Chandrasekhar, Appl. Phys. Lett. 66, 1095 (1995).
[g] F. Capasso, K. Mohammed, K. Alavi, A. Y. Cho and P. W. Foy, Appl. Phys. Lett. 45, 968 (1984).

[b]T. P. Pearsall, R. E. Nahory and M. A. Pollack, Appl. Phys. Lett. 28, 403 (1976).
[i]H. Kuwatsuka, T. Mikawa, S. Miura, N. Yasuoka, T. Tanahashi , O. Wada, Appl. Phys. Lett. 57, 249 (1990).
[j] H. D. Law and C. A. Lee, Solid State Electron. 21, 331 (1978).
[k]J.P.R. David, M. Hopkinson and M.A. Pate, Electron. Lett. 30, 909 (1994).

Table V

material	E_g	$<E_c>$	V_b
	(eV)	(eV)	(V)
Si	1.17	1.85	38.7
BN	5.81	8.96	364.2
BP	2.04	3.34	107.1
B_As	1.55	2.72	78.4
AlN	4.54	6.52	252.7
GaN	3.25	4.79	173.3
AlP	2.50	3.24	102.4
AlAs	2.23	2.41	64.3
AlSb	1.68	2.09	49.6
GaP	2.39	2.58	72.1
GaAs	1.52	1.77	35.0
InP	1.42	2.09	49.6
InAs	0.41	1.51	(23.2)
$In_{0.53}Ga_{0.47}As$	0.81	1.68	30.6
ZnS	3.80	4.65	166.9
ZnSe	2.96	3.78	127.1
ZnTe	2.71	2.97	90.1
CdS	2.55	4.30	150.8
CdSe	1.90	3.56	116.7
CdTe	1.92	2.78	81.1
HgTe	0.00	1.49	(22.2)

Table VI

substrate	a_0	Material	$<E_c>$	V_b*
	Å		(eV)	(V)
GaAs	5.6532	GaAs	1.77	34.8
		$Ga_{0.52}In_{0.48}P$	2.34	60.9
		$Al_{0.52}In_{0.48}P$	2.70	77.4
		$GaP_{0.69}Sb_{0.31}$	2.09	49.5
		$AlP_{0.70}Sb_{0.30}$	2.90	86.6

* Breakdown voltage of 1µm p-i-n diode. calculated from Equation (9)

Table VI (continued)

substrate	a_0 Å	Material	$<E_c>$ (eV)	V_b* (V)
InP	5.8688	InP	2.09	49.5
		$In_{0.53}Ga_{0.47}As$	1.65	29.3
		$Al_{0.48}In_{0.52}As$	1.96	43.5
		$GaAs_{0.51}Sb_{0.49}$	(1.39)	(17.4)
		$GaP_{0.36}Sb_{0.65}$	1.55	24.7
		$AlAs_{0.56}Sb_{0.44}$	2.27	57.7
		$AlP_{0.39}Sb_{0.61}$	2.54	70.1
InAs	6.0584	InAs	(1.51)	(22.9)
		$GaAs_{0.08}Sb_{0.92}$	(1.05)	(1.8)
		$GaP_{0.06}Sb_{0.94}$	(1.09)	(3.7)
		$InP_{0.69}Sb_{0.31}$	1.76	34.4
		$AlAs_{0.16}Sb_{0.84}$	2.14	51.8
		$AlP_{0.11}Sb_{0.89}$	2.22	55.4
GaSb	6.0959	GaSb	(0.99)	(-)
		$InAs_{0.91}Sb_{0.09}$	(1.47)	(21.1)
		$InP_{0.63}Sb_{0.37}$	1.70	31.6
		$AlAs_{0.08}Sb_{0.92}$	2.12	50.4
		$AlP_{0.06}Sb_{0.94}$	2.16	52.7

* Breakdown voltage of 1μm p-i-n diode, calculated from Equation (9)

Claims

1. A method of forming a semiconductor structure comprising forming the structure such that the Brillouin-zone-averaged energy bandgap ($< E_c >$) of at least a portion (2, 13, 15, 23, 32, 39, 44, 54, 58) of thereof is controlled on the basis of a desired avalanche breakdown characteristic therefor.

2. A method according to claim 1, wherein the predetermined avalanche characteristic is avalanche breakdown voltage (V_b).

3. A method according to claim 1 or 2, wherein said portion (2, 13, 23, 32, 39, 44, 54, 58) of the structure is formed from a material selected on the basis of its Brillouin-zone-averaged energy bandgap ($< E_c >$).

4. A method according to claim 1 or 2 wherein said portion of the structure is formed of an alloy with a predetermined value of $< E_c >$.

5. A method according to claim 1 or 2 wherein said portion of the structure is formed of a strained layer or a strained layer superlattice such that a predetermined value of $< E_c >$ is established by the strain.

6. A method according to claim 5 wherein the strain is selected on the basis of a desired avalanche breakdown characteristic.

7. A method according to claim 1 or 2 including forming said portion of the structure so as to be spatially compositionally graded in a predetermined manner in terms of $< E_c >$.

8. A method according to claim 1 or 2 including forming said portion of the structure as a superlattice pseudoalloy.

9. A method according to claim 1 or 2 including forming said portion of the structure as a multiple quantum well structure (L1, L2).

10. A method according to any preceding claim, wherein the structure is formed such that the bandgap (E_g) of said portion of the structure has a predetermined value.

11. A method according to any one of claims 1 to 11 wherein said Brillouin-zone-averaged energy bandgap of said portion is selected according to the following relationship:

$$<E_c> = \frac{(V_b + m)}{n}$$

where V_b is a predetermined breakdown voltage, and m and n are constants.

12. A method according to any one of claims 1 to 11 wherein the structure comprises a FET including a source (7) and a drain (8), and said portion of the structure comprises a channel layer (2) for providing a conduction path between the source and the drain, including forming the channel layer such that the value of $< E_c >$ thereof increases between the source and drain.

13. A method according to claim 12 including forming the channel with a predetermined grading of $< E_c >$.

14. A method according to claim 12 including forming the channel of first and second portions (2a, 2b) with different values of $< E_c >$.

15. A method according to claim 12, 13 or 14 including forming the channel (12) as a strained layer.

16. A method according to any one of claims 12 to 15 including forming a channel (15) on a semiconductor substrate (1), forming a further semiconductor layer (16) overlying the channel, forming a V-groove (17) into the substrate, through the channel, forming source gate and drain regions (18, 19, 20) on a side of the V-groove.

17. A method according to claim 12 including forming layers (13) of successively larger values of average energy on a substrate to produce a multi-layer structure, cleaving the multi-layer structure to expose ends of the layers, and forming a source electrodes (4), a gate electrode (6) and a drain electrode (5) over said ends.

18. A method according to any one of claims 1 to 11 wherein the structure comprises an APD.

19. A method according to claim 18 including forming a light absorption region (32) for producing carriers in response to optical radiation and a multiplication region (31) for producing further charge carriers by avalanche multiplication, including configuring the $< E_c >$ for the absorption region to be greater than that for the multiplication region.

20. A method according to claim 19 including configuring the value of E_g for the absorption region (32) and the multiplication region (31) such that there is substantially no discontinuity in the conduction and valance bands E_c, E_v at the junctions between the regions.

21. A method according to any one of claims 18 to 20 including forming an absorption and multiplication layer as superlattice (30) of materials selected to produce photocarriers in response to optical radiation at a predetermined wavelength and to have a predetermined value of $< E_c >$ for producing charge carrier avalanche multiplication.

22. A method according to any one of claims 18 to 20 including forming an absorption layer (39) as a superlattice of materials selected to produce photocarriers in response to optical radiation at a predetermined wavelength, and a multiplication layer (44) for producing charge carrier multiplication, the value of $< E_c >$ for the absorption layer (39) being selected to be greater than that for the multiplication layer.

23. A method according to any one of claims 1 to 11 wherein the structure comprises an IMPATT device.

24. A method according to any one of claims 1 to 11 wherein the structure comprises a bipolar transistor.

25. A method according to claim 11, wherein the structure is a p-i-n diode having a 1μm wide i region, m is approximately 45.8 and n is approximately 46.3.

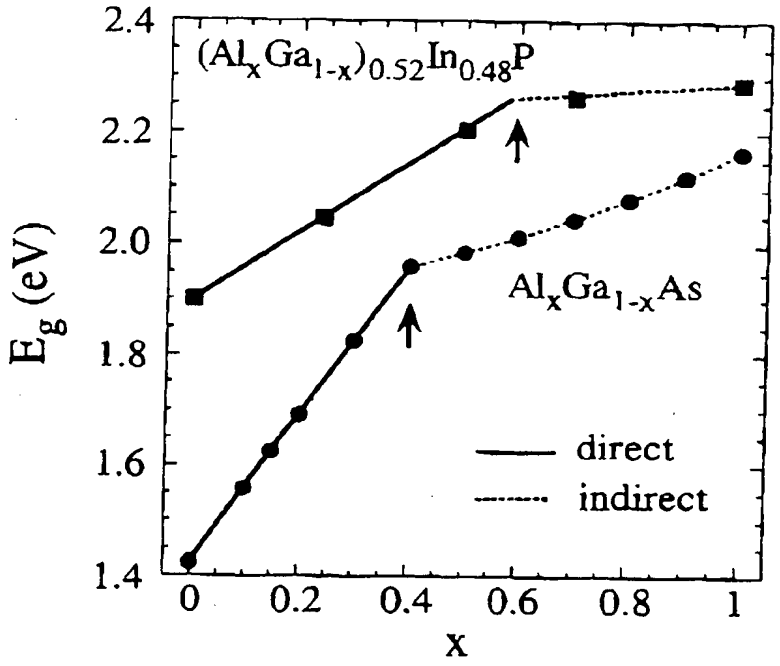

(a)

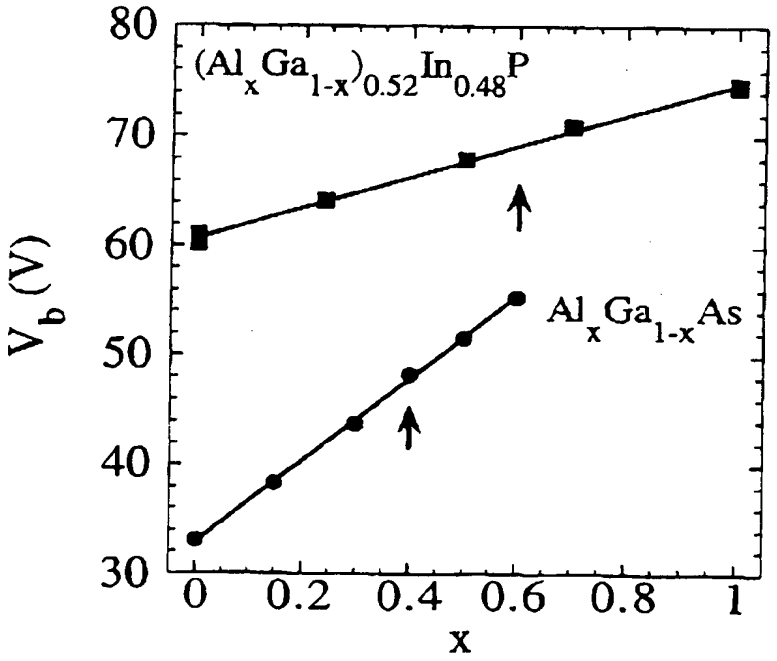

(b)

FIG. 1

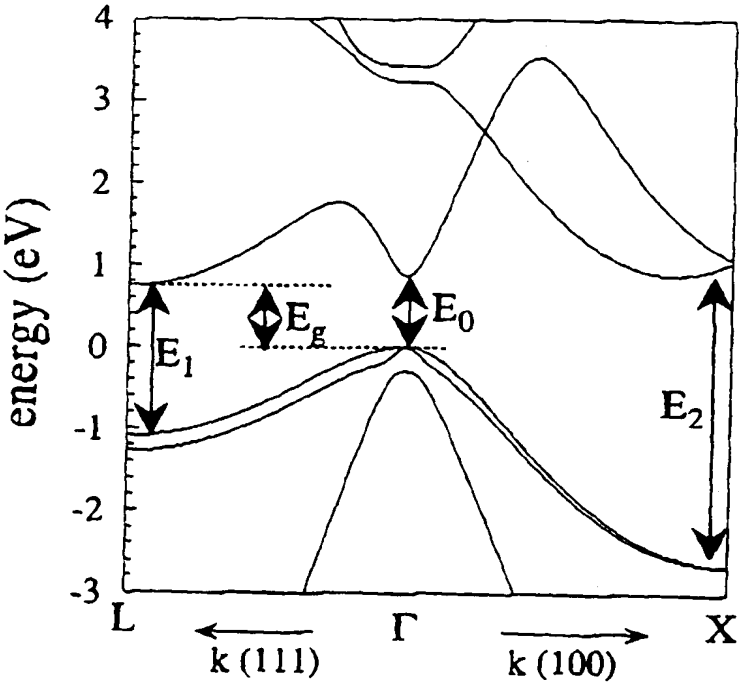

(a)

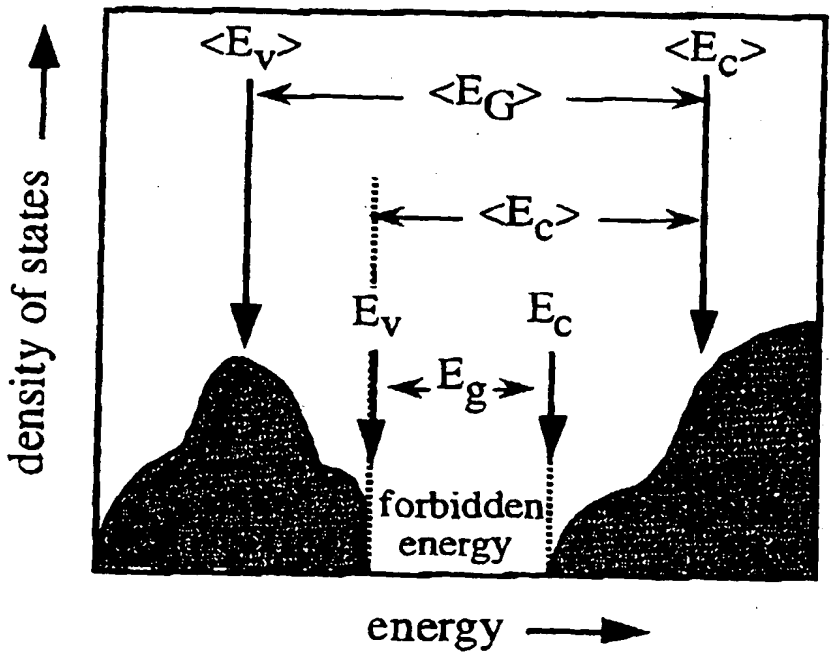

(b)

FIG. 2.

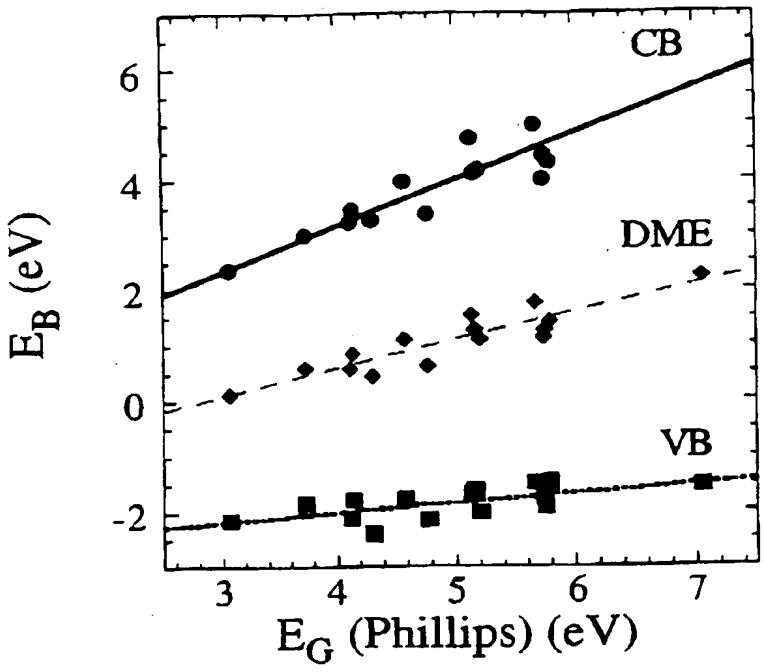

(a)

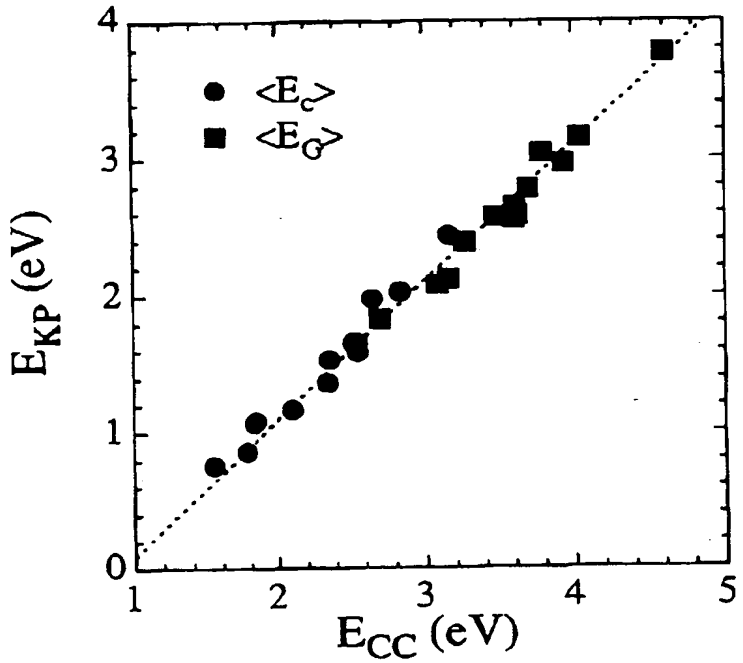

(b)

FIG. 3

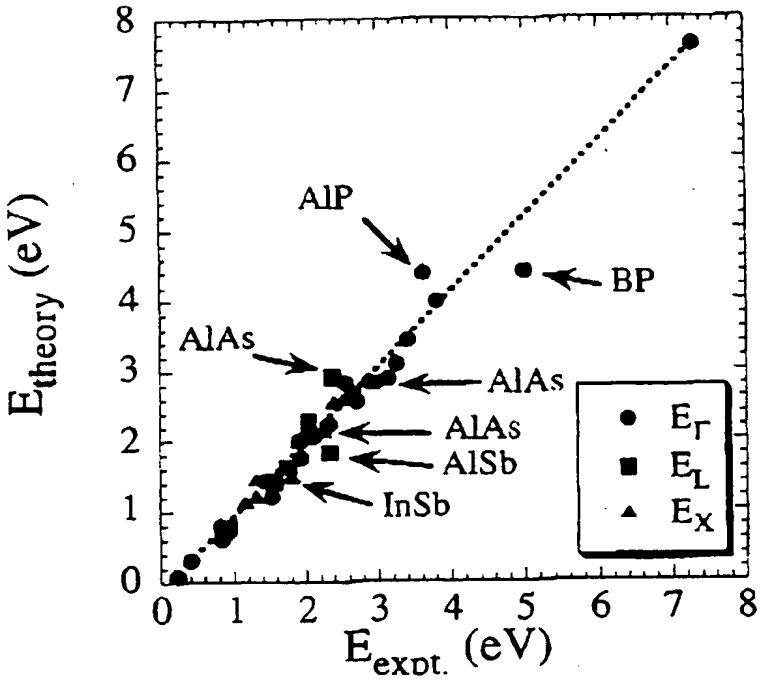

(a)

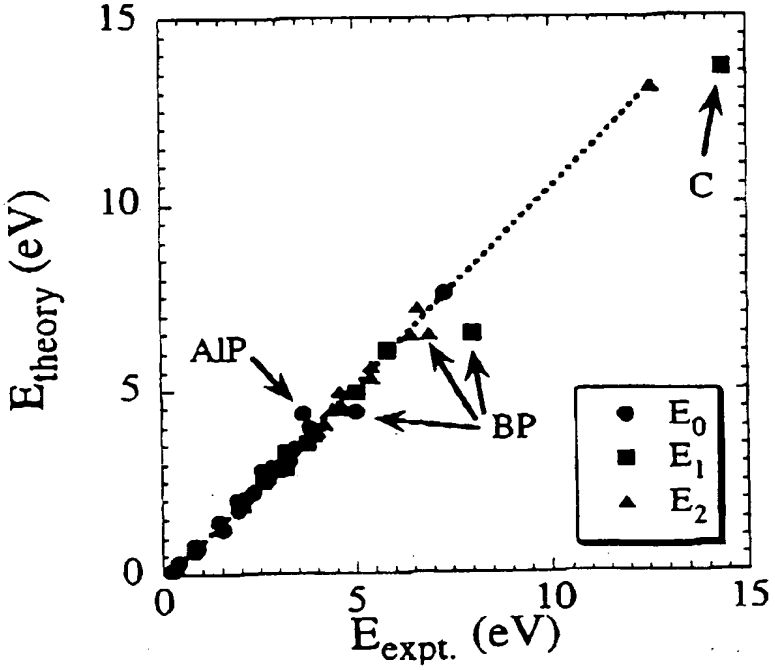

(b)

FIG. 4

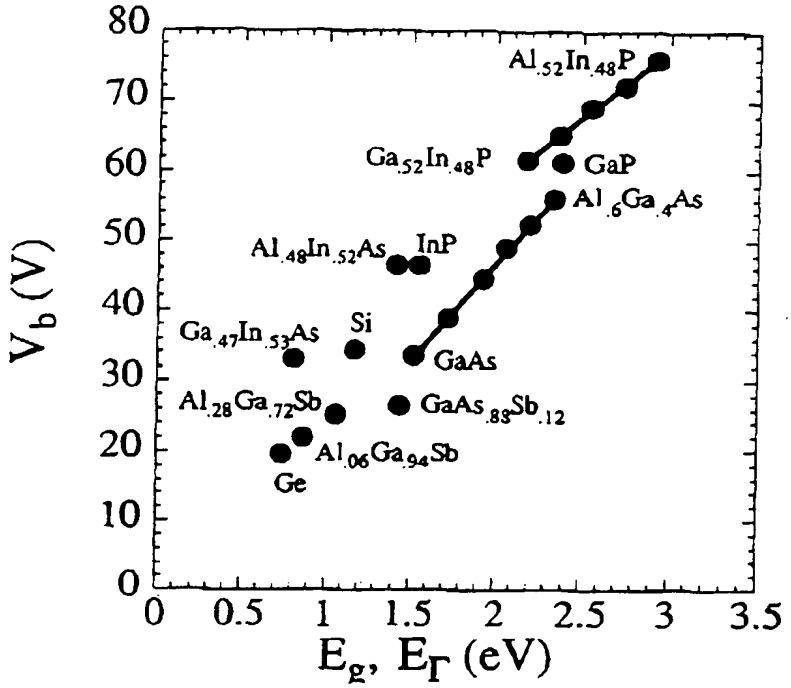

(a)

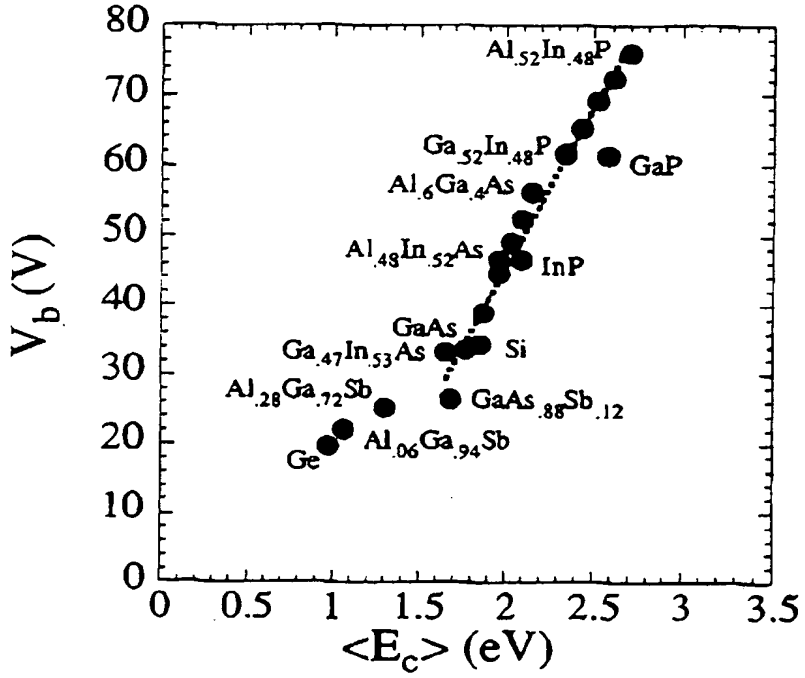

(b)

FIG. 5

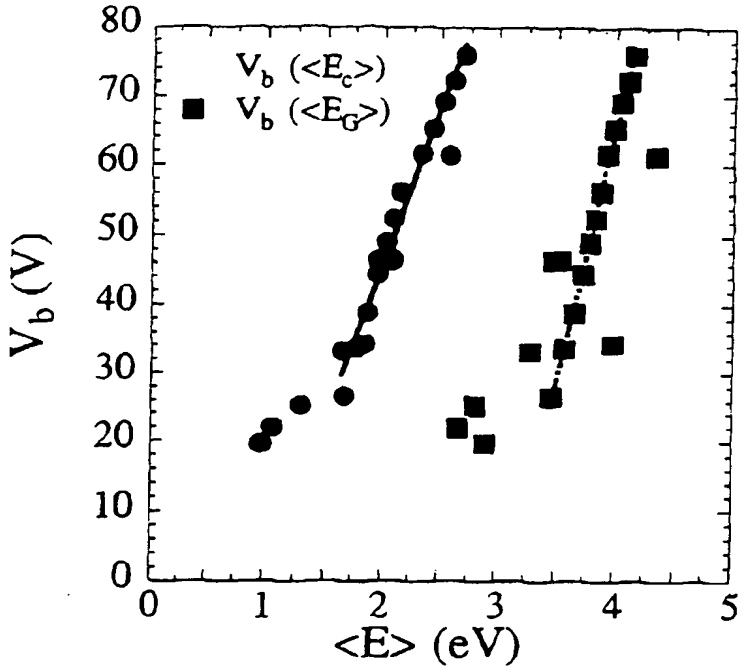

(a)

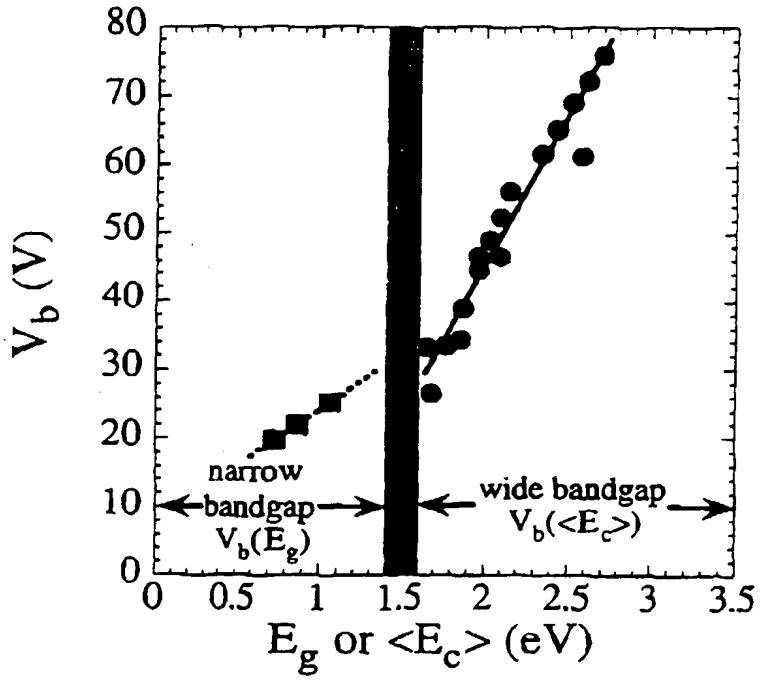

(b)

FIG. 6

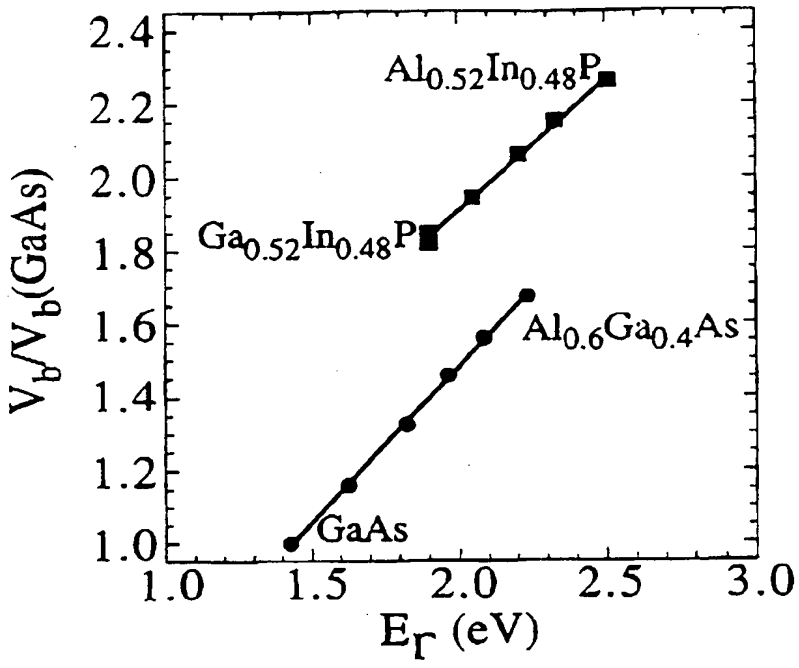

(a)

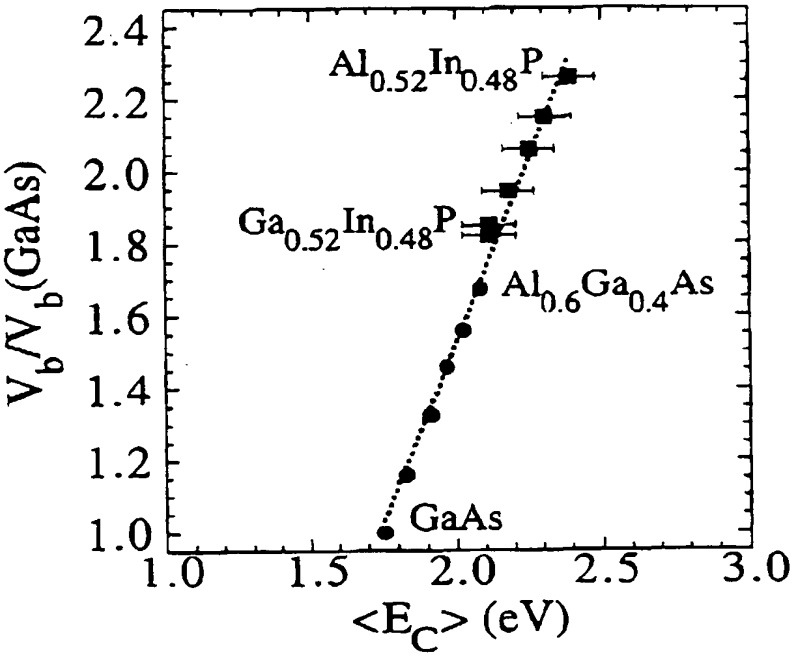

(b)

FIG. 7

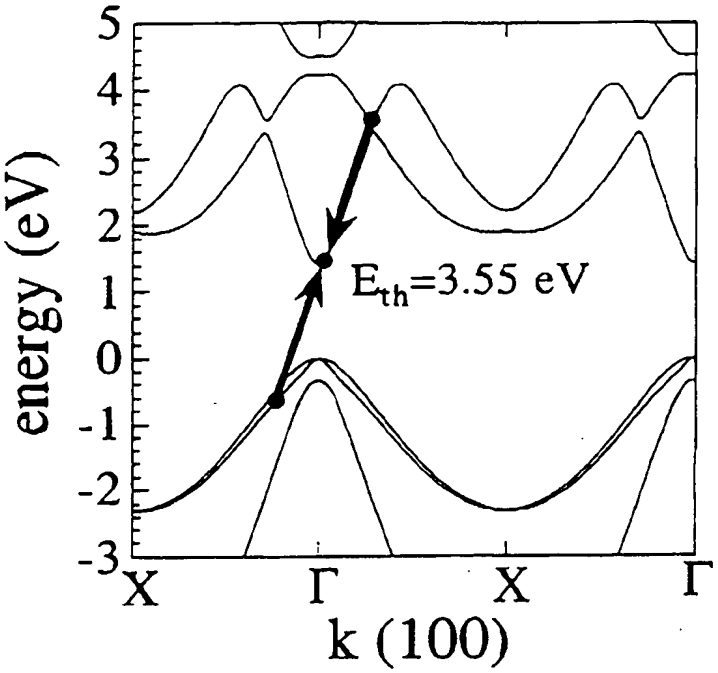

(a)

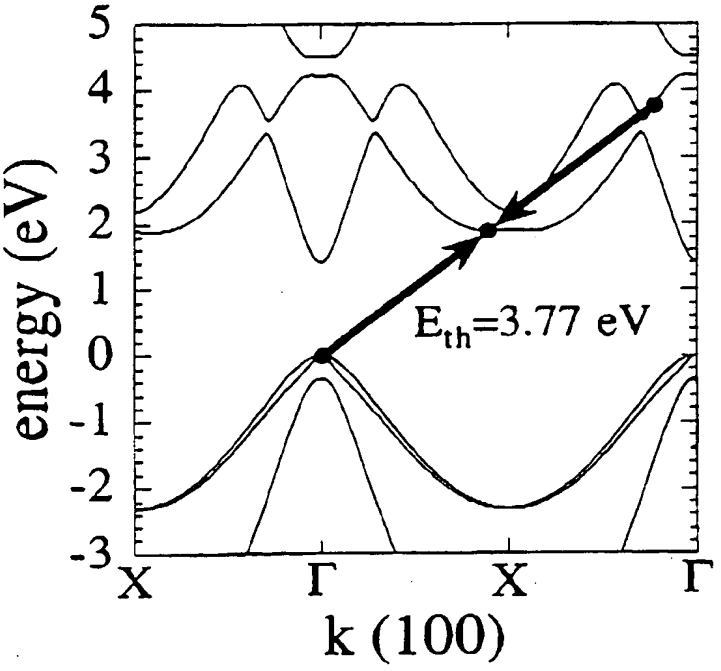

(b)

FIG. 8

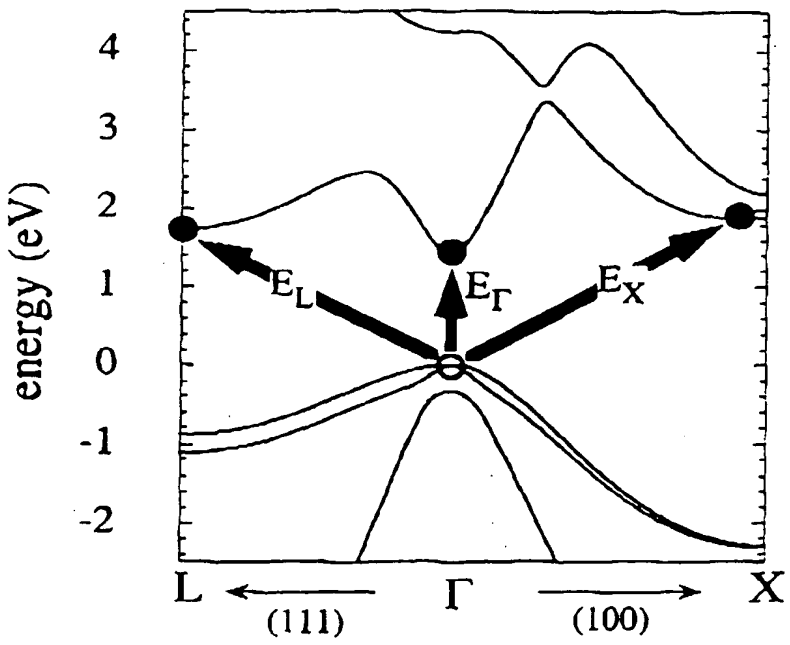

(a)

Valley	Degeneracy
Γ (000)	1
X (100)	3
L (111)	4

(b)

FIG. 9.

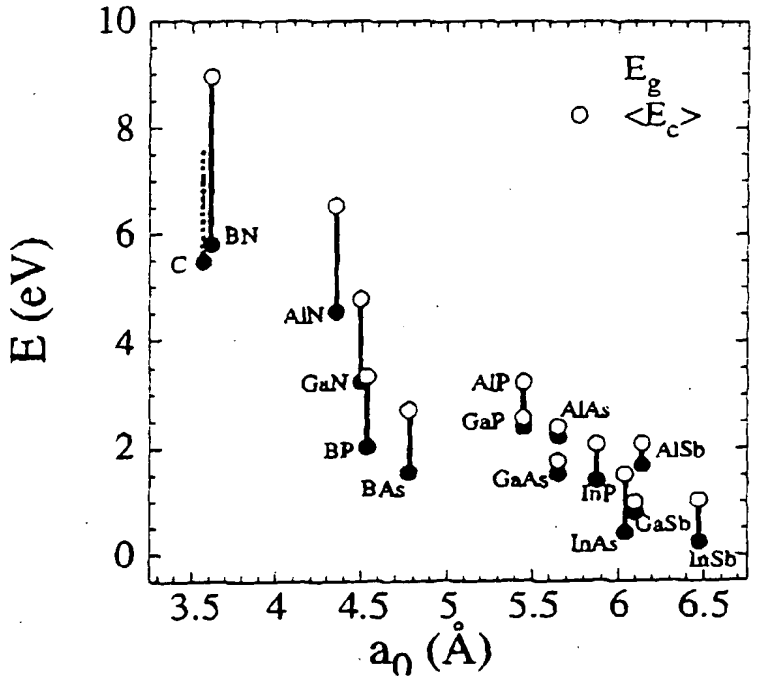

(a)

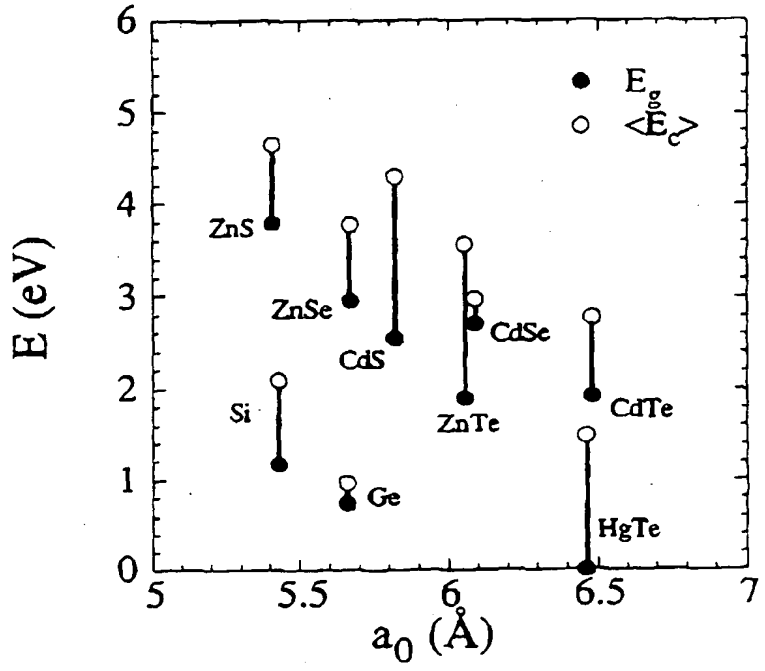

(b)

FIG. 11

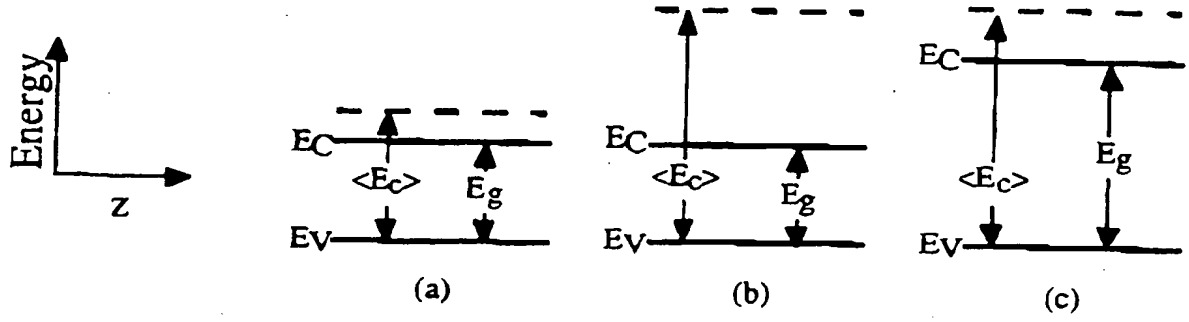

FIG. 10

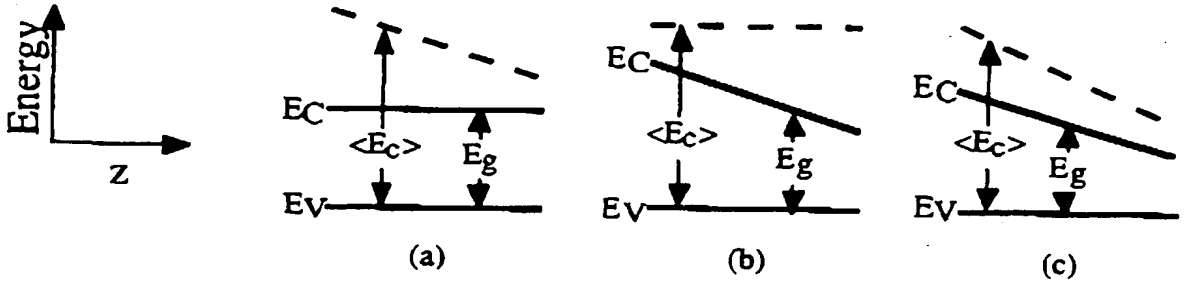

FIG. 12

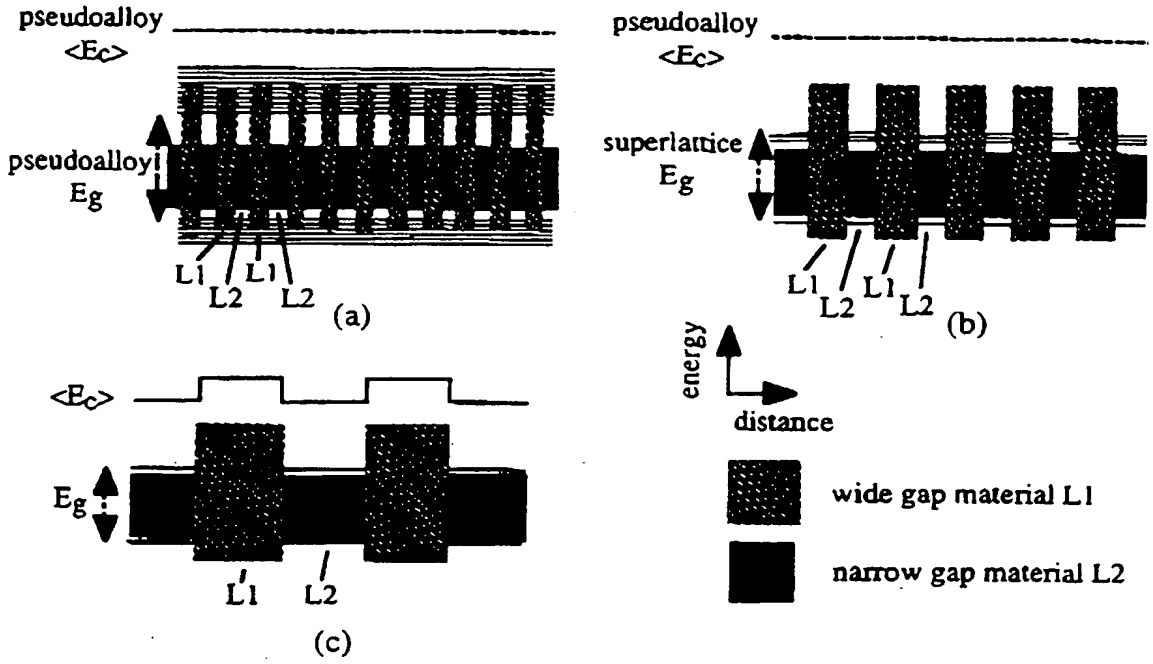

FIG. 13

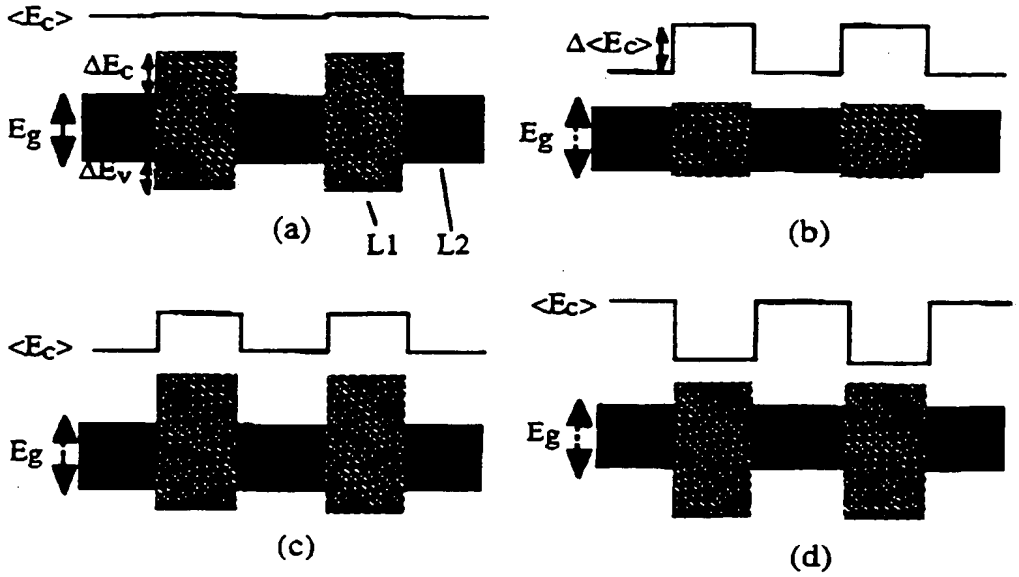

FIG. 14

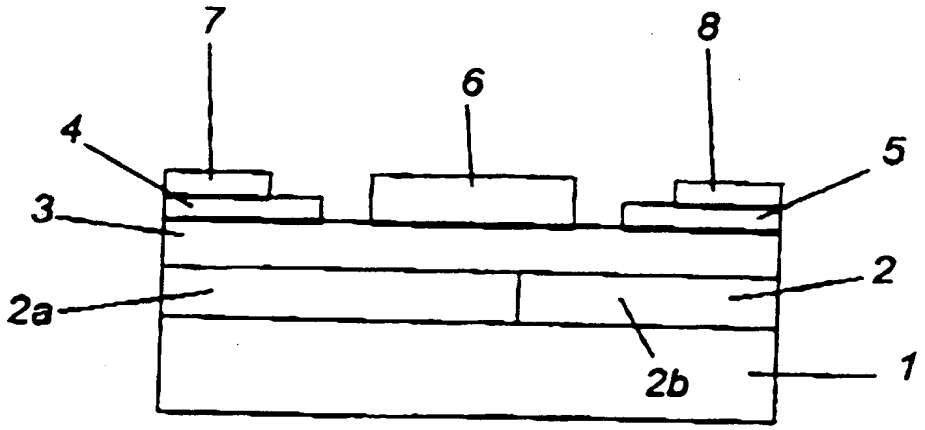

Fig. 15

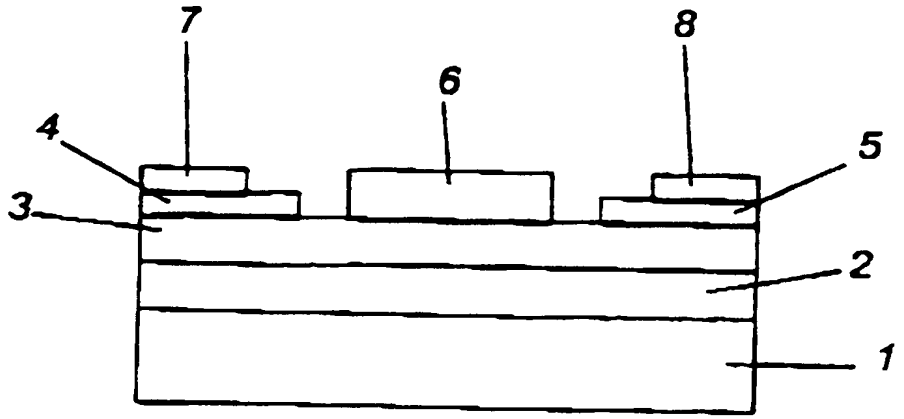

Fig. 16

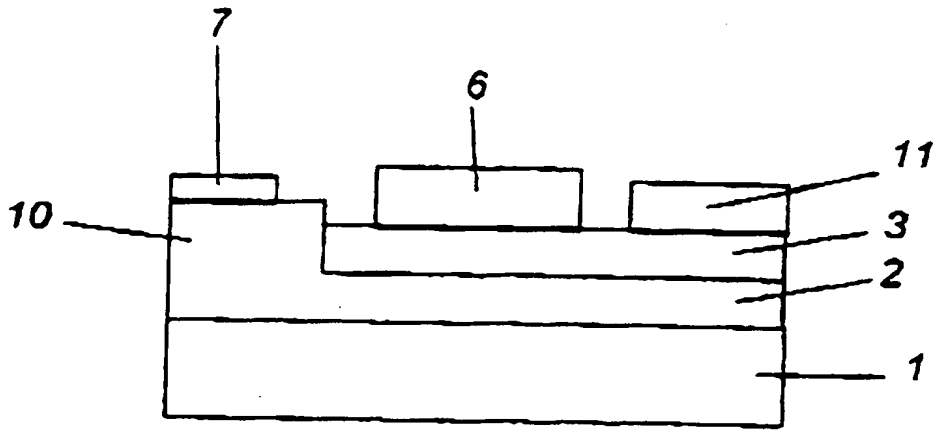

Fig. 17

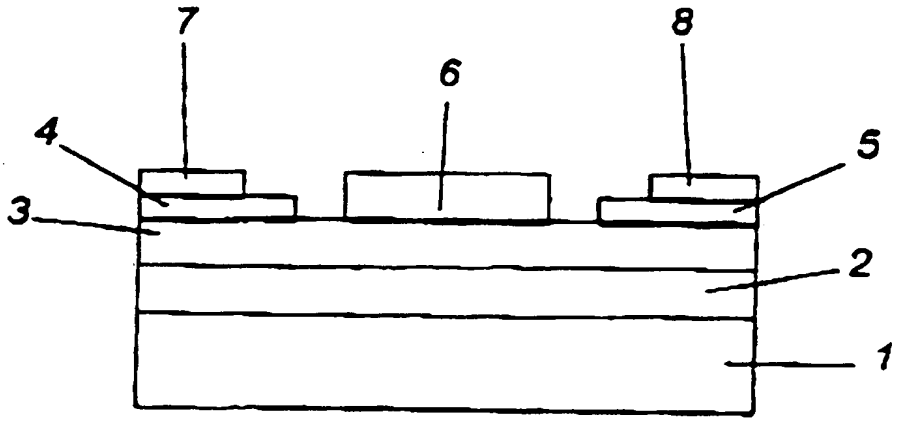

Fig. 18

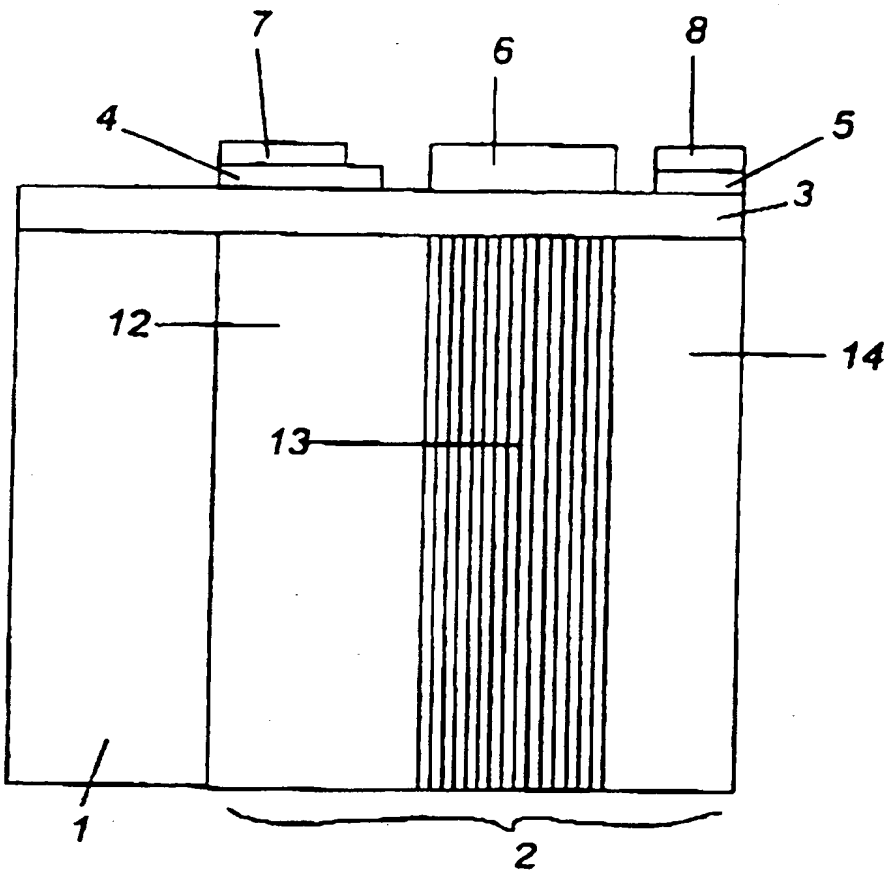

Fig. 19

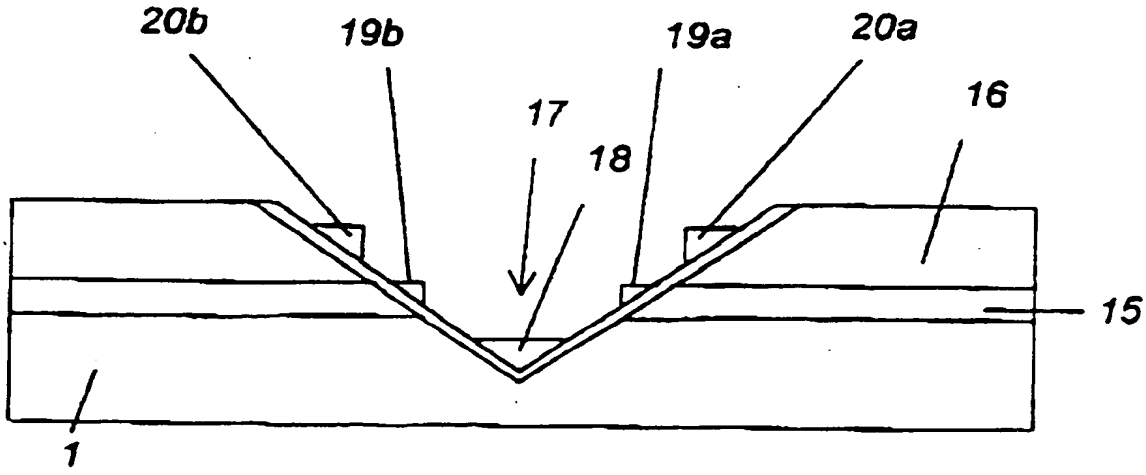

Fig. 20

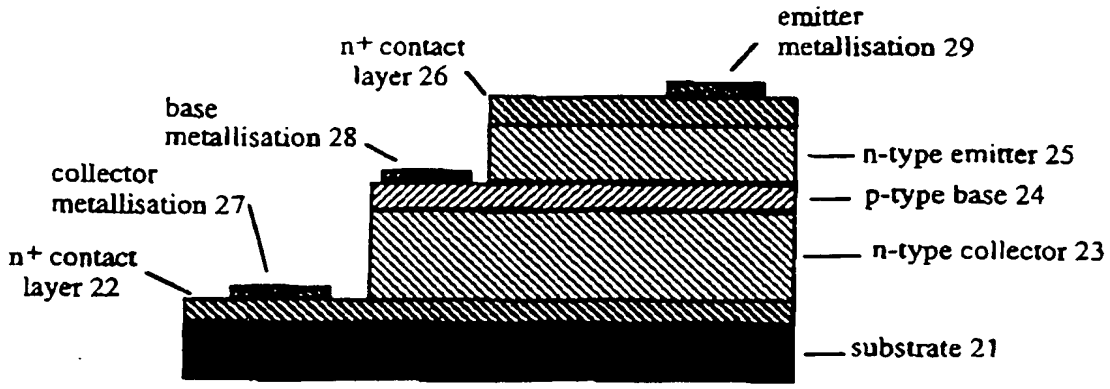

FIG. 21

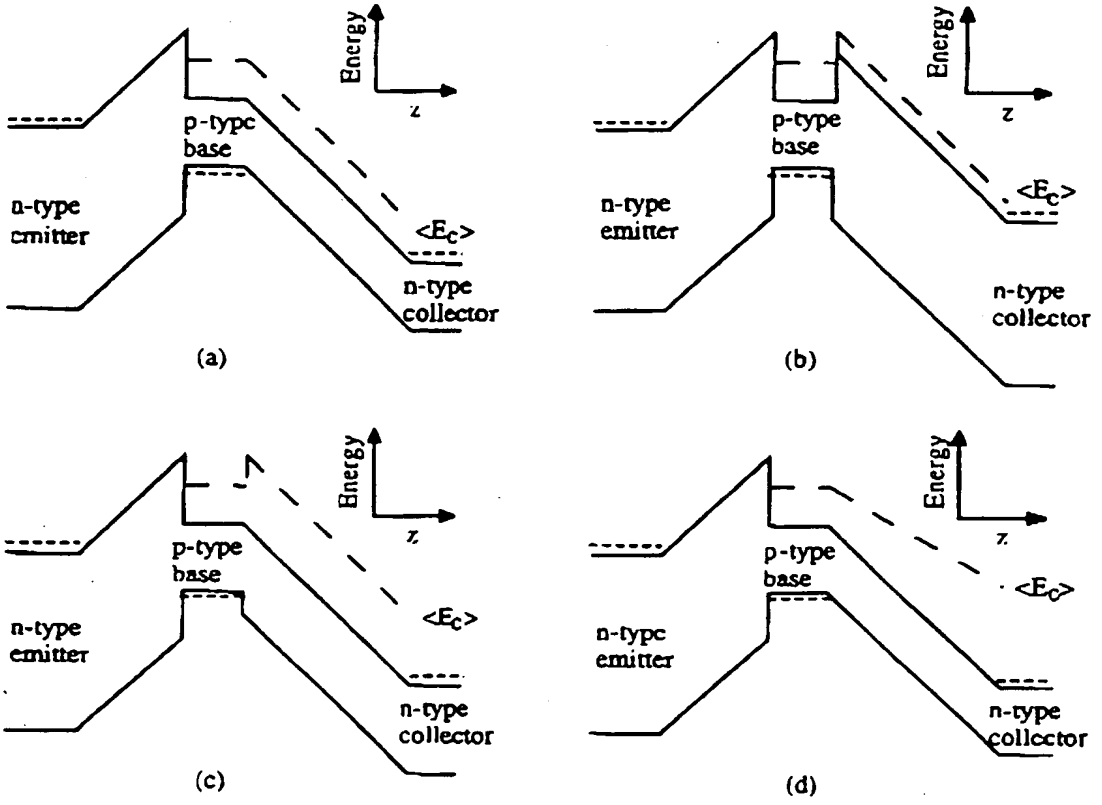

FIG. 22

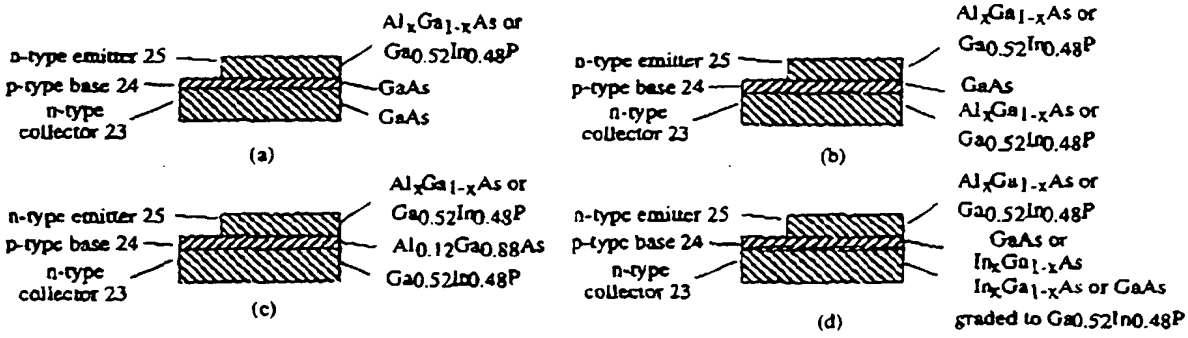

FIG. 23

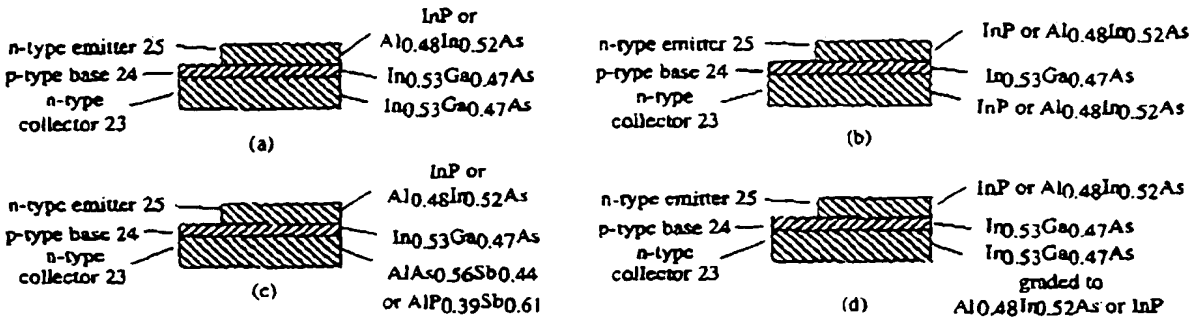

FIG. 24

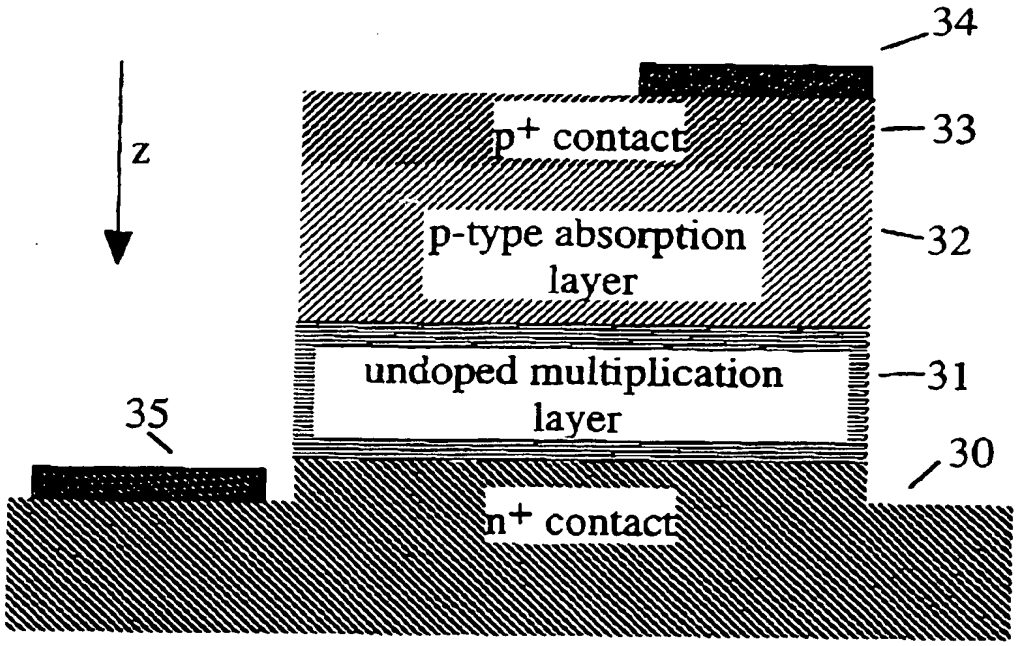

FIG. 25

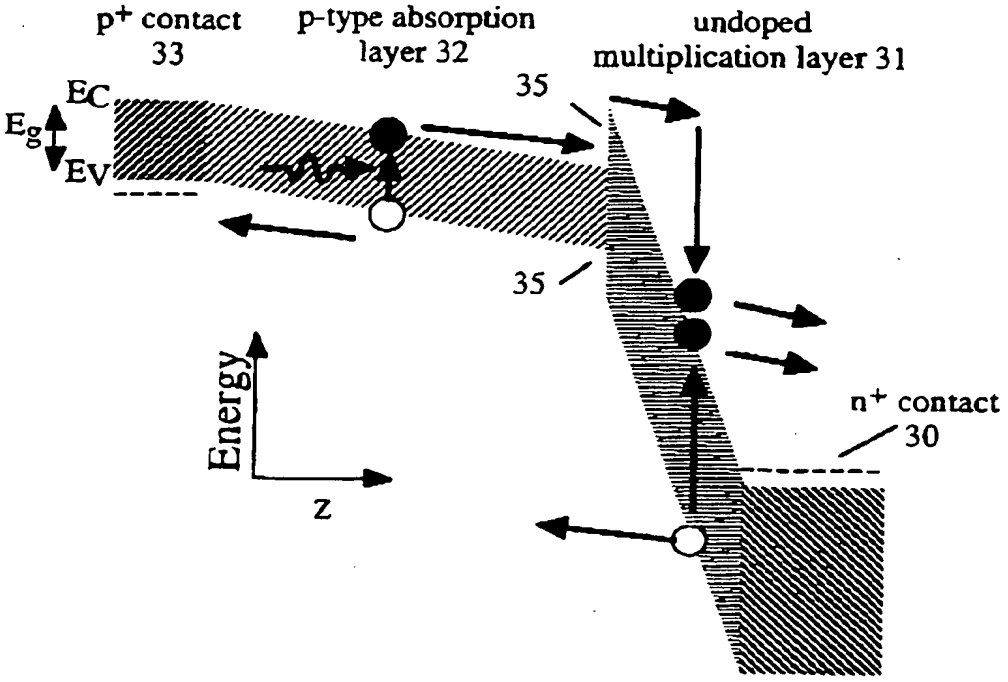

FIG. 26

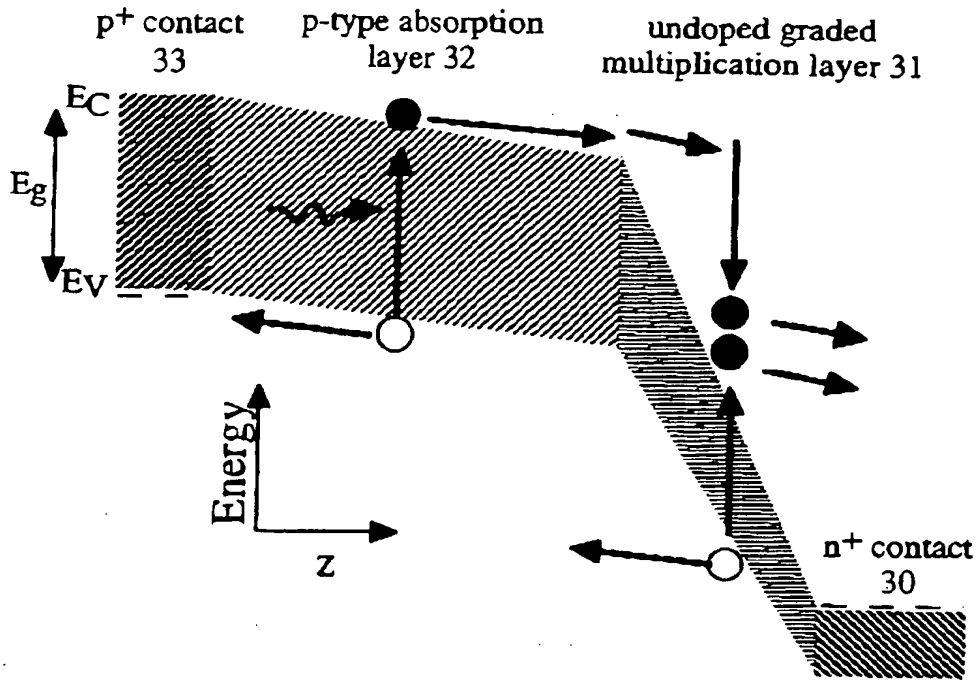

FIG. 27

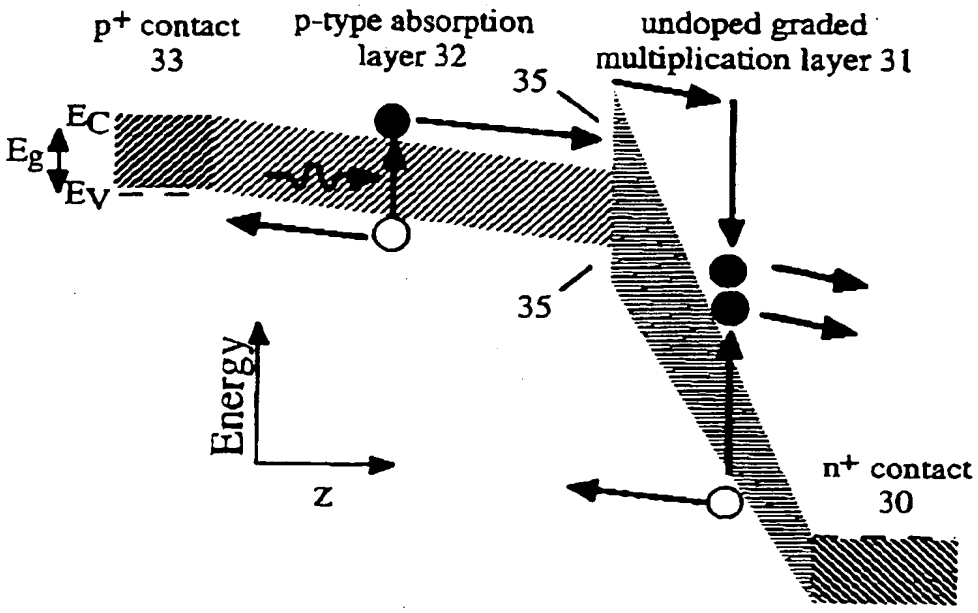

FIG. 28

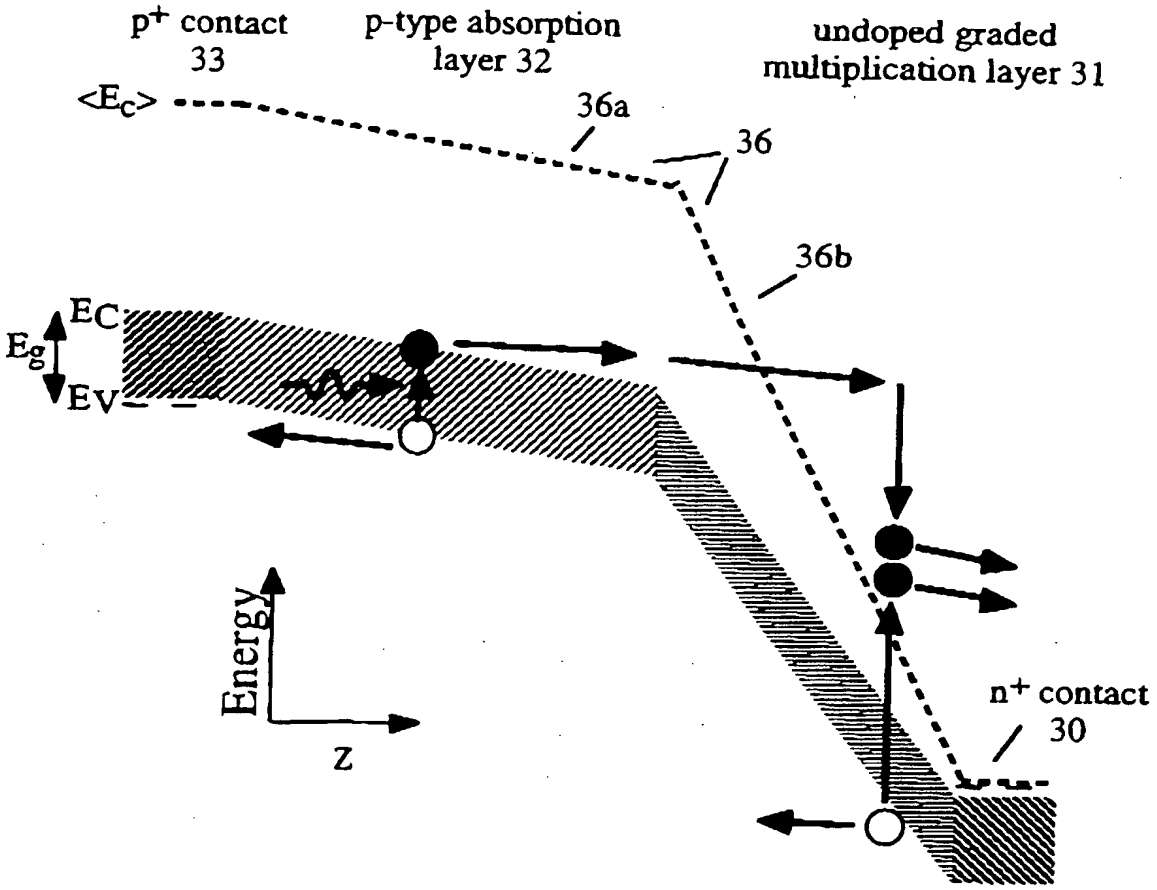

FIG. 29

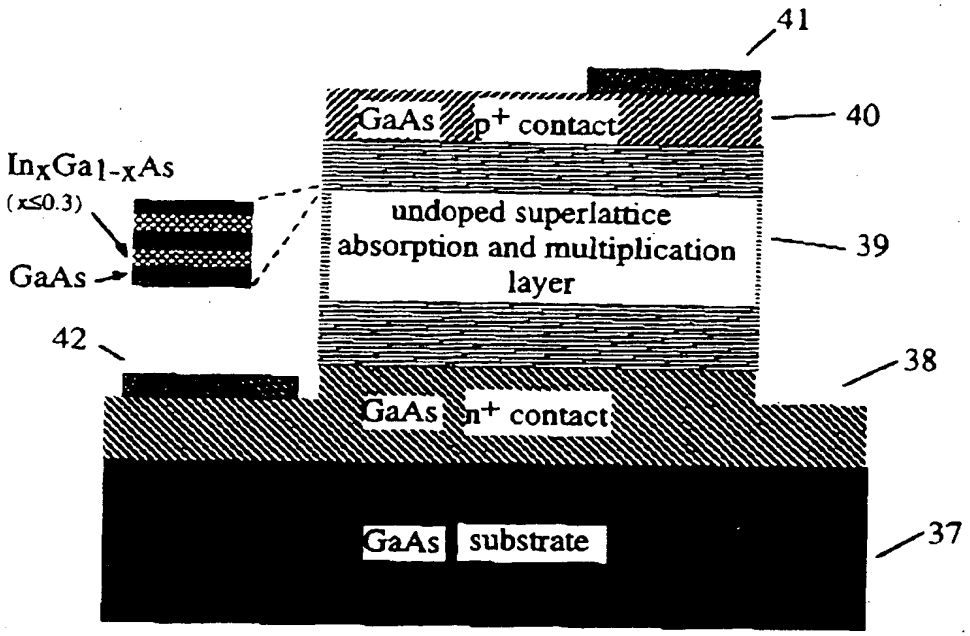

FIG. 30

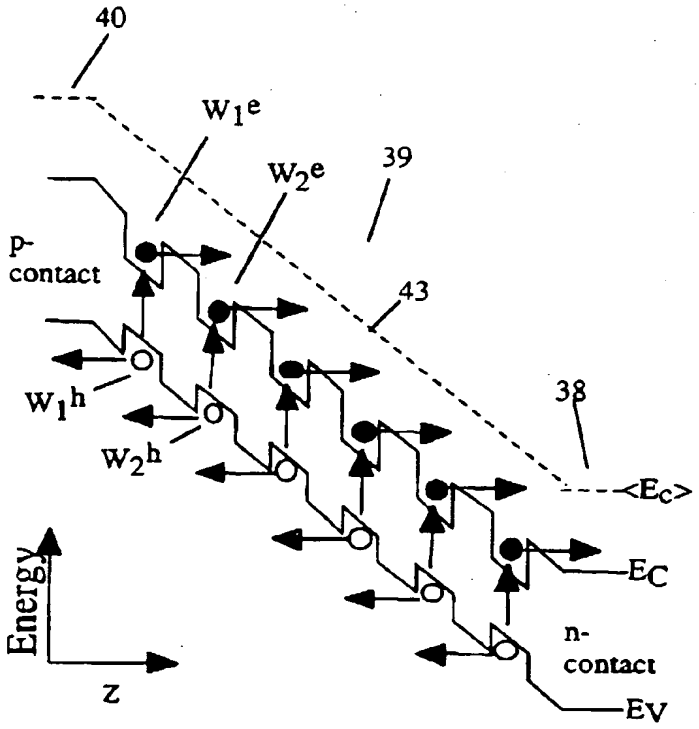

FIG. 31

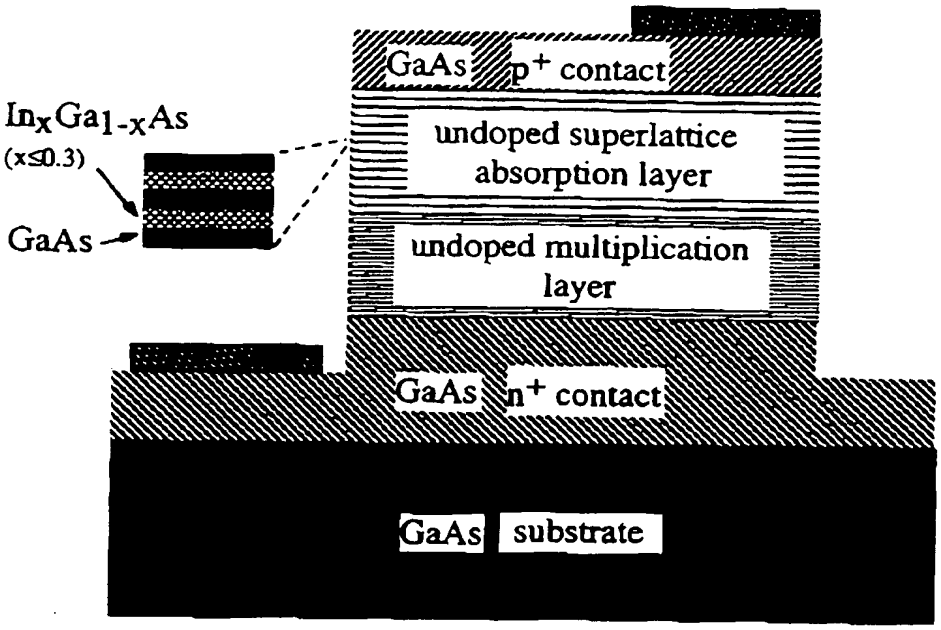

FIG. 32

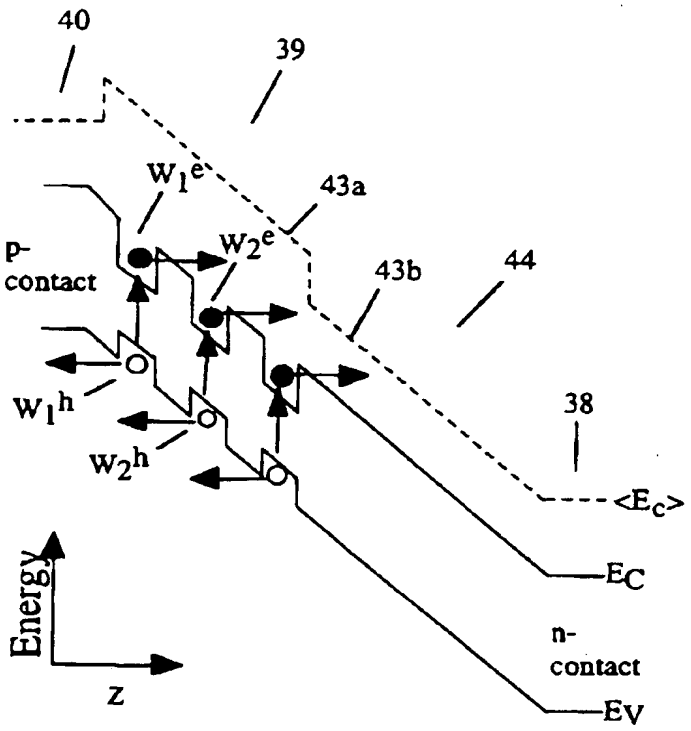

FIG. 33

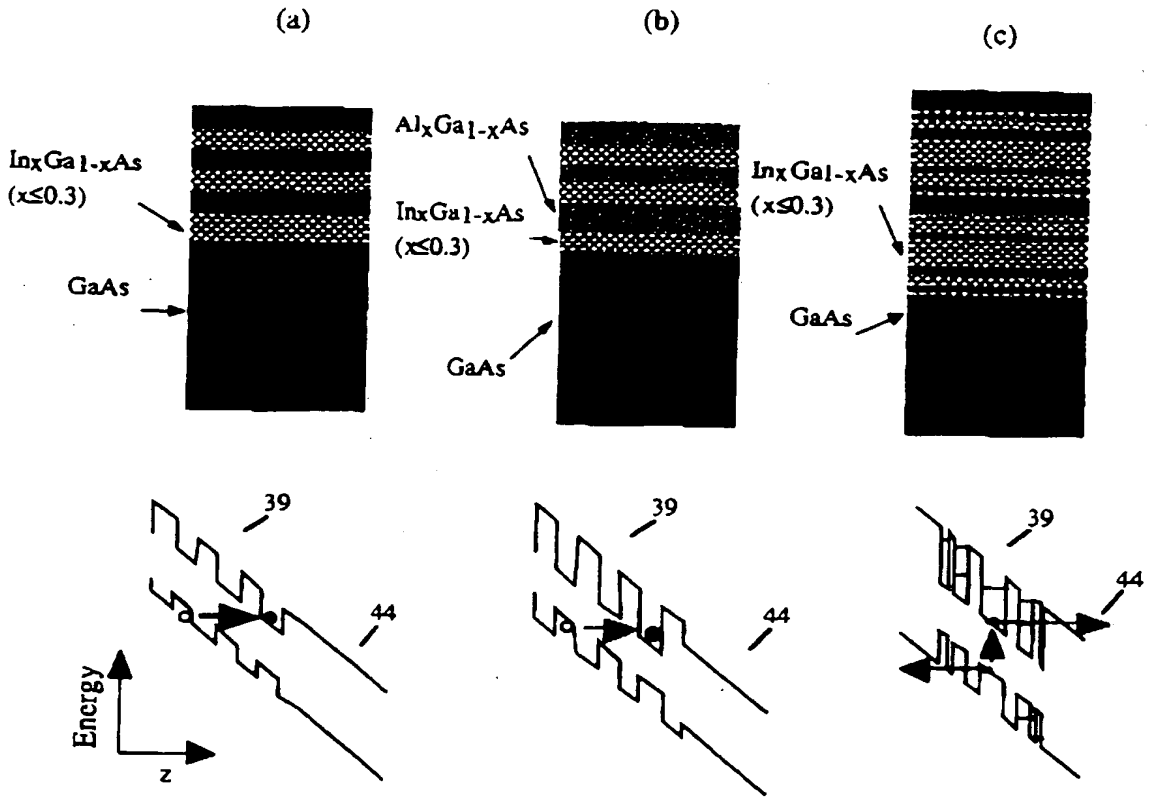

FIG. 34

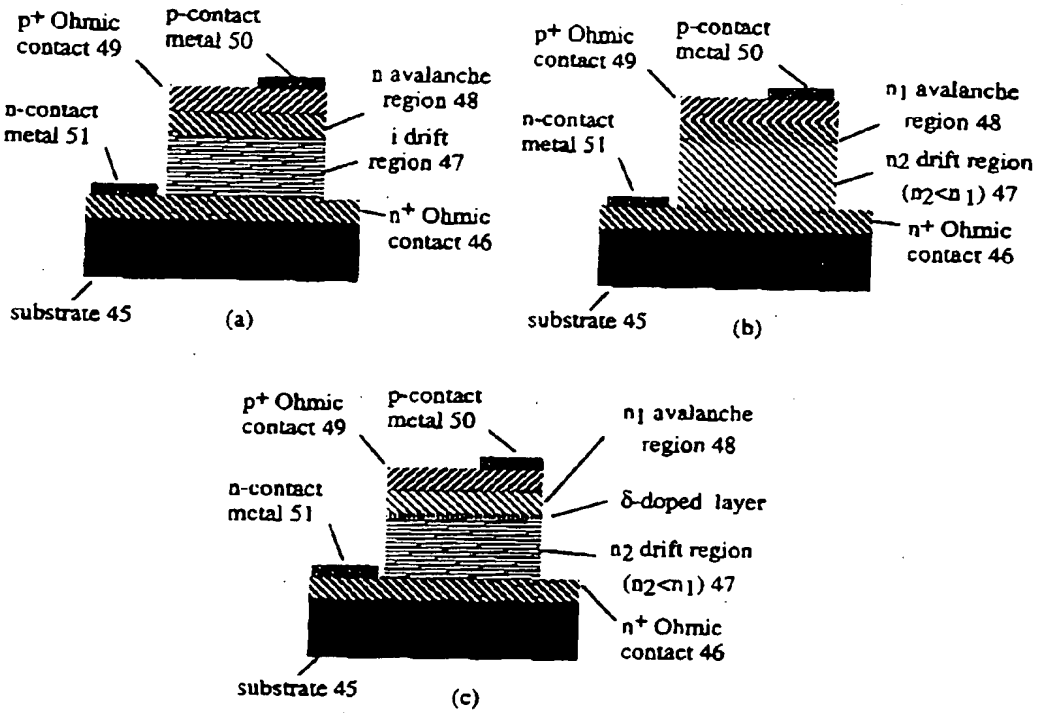

FIG. 35

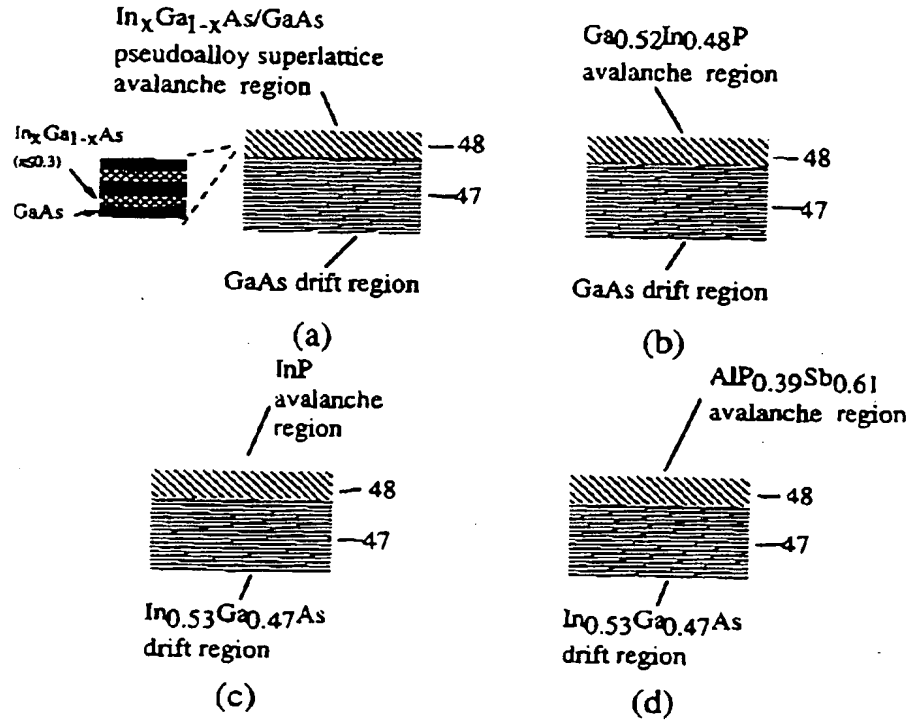

FIG. 36

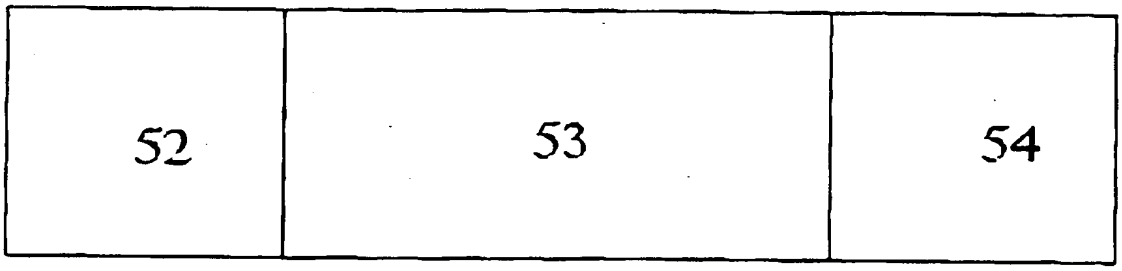

FIG. 37

European Patent Office

PARTIAL EUROPEAN SEARCH REPORT

which under Rule 45 of the European Patent Convention shall be considered, for the purposes of subsequent proceedings, as the European search report

Application Number EP 96 30 5577

DOCUMENTS CONSIDERED TO BE RELEVANT

Category	Citation of document with indication, where appropriate, of relevant passages	Relevant to claim	CLASSIFICATION OF THE APPLICATION (Int.Cl.6)
D,A	GB-A-2 084 797 (WESTERN ELECTRIC COMPANY INCORPORATED)		H01L29/868 H01L31/075 H01L29/12 H01L29/864 H01L29/737 H01L29/778
A	SOLID STATE DEVICES 1983. 13TH EUROPEAN SOLID STATE DEVICE RESEARCH CONFERENCE (ESSDERC), no. 69, 13 - 19 September 1983, CANTERBURY, GB, pages 15-28, XP002019202 N.T. LINH: "Superlattices and electron devices"		
A	SOLID STATE ELECTRONICS, vol. 11, no. 10, October 1968, OXFORD GB, pages 917-932, XP002019203 C.Y. DUH ET AL.: "Temperature dependance of hot electron drift velocity in silicon at high electric field"		

-/--

TECHNICAL FIELDS SEARCHED (Int.Cl.6)

H01L

INCOMPLETE SEARCH

The Search Division considers that the present European patent application does not comply with the provisions of the European Patent Convention to such an extent that it is not possible to carry out a meaningful search into the state of the art on the basis of some of the claims

Claims searched completely :

Claims searched incompletely : 1-25

Claims not searched :

Reason for the limitation of the search:

see sheet C

Place of search	Date of completion of the search	Examiner
THE HAGUE	22 November 1996	Baillet, B

CATEGORY OF CITED DOCUMENTS

X : particularly relevant if taken alone
Y : particularly relevant if combined with another document of the same category
A : technological background
O : non-written disclosure
P : intermediate document

T : theory or principle underlying the invention
E : earlier patent document, but published on, or after the filing date
D : document cited in the application
L : document cited for other reasons

& : member of the same patent family, corresponding document

EPO FORM 1503 03.82 (P04C07)

European Patent Office

PARTIAL EUROPEAN SEARCH REPORT

Application Number
EP 96 30 5577

DOCUMENTS CONSIDERED TO BE RELEVANT			CLASSIFICATION OF THE APPLICATION (Int.Cl.6)
Category	Citation of document with indication, where appropriate, of relevant passages	Relevant to claim	
D,A	ELECTRONICS LETTERS, vol. 16, no. 12, 5 June 1980, STEVENAGE GB, pages 467-469, XP002019204 R. CHIN ET AL.: "Impact ionisation in multulayered heterojunction structures" ---		
A	PATENT ABSTRACTS OF JAPAN vol. 9, no. 178 (E-330), 23 July 1985 & JP-A-60 049681 (FUJITSU KK), 18 March 1985, * abstract * ---		
A	US-A-4 799 087 (MATSUYAMA ET AL.) -----		TECHNICAL FIELDS SEARCHED (Int.Cl.6)

EPO FORM 1503 03.82 (P04C10)

EP 96305577.7

- C -

Reason for the limitation of the search:

A complete search can not be done for claim 1, because it discloses a very broad and general concept. Hence, the other claims depending from claim 1 can not be completely searched.